Bioorganic Chemistry 131 (2023) 106334

Contents lists available at ScienceDirect

Bioorganic Chemistry

journal homepage: www.elsevier.com/locate/bioorg

Triazole-based estradiol dimers prepared *via* CuAAC from 17α-ethinyl estradiol with five-atom linkers causing G2/M arrest and tubulin inhibition

Michal Jurášek [a], Jiří Řehulka [b], Lenka Hrubá [b], Aleksandra Ivanová [b], Soňa Gurská [b], Olena Mokshyna [b], Pavel Trousil [a], Lukáš Huml [a], Pavel Polishchuk [b], Marián Hajdúch [b], Pavel B. Drašar [a], Petr Džubák [b,*]

[a] *Department of Chemistry of Natural Compounds, University of Chemistry and Technology Prague, Technická 5, 166 28 Prague 6, Czech Republic*
[b] *Institute of Molecular and Translational Medicine, Faculty of Medicine and Dentistry, Palacký University and University Hospital in Olomouc, Hněvotínská 1333/5, 779 00 Olomouc, Czech Republic*

ARTICLE INFO

Keywords:
Steroid dimer
Estradiol
Chemistry
CuAAC reaction
Cytotoxicity
Cell cycle
G2/M arrest
Microtubules
Antimitotic activity
Tubulin assembly
In silico simulations

ABSTRACT

Microtubule dynamic is exceptionally sensitive to modulation by small-molecule ligands. Our previous work presented the preparation of microtubule-targeting estradiol dimer (ED) with anticancer activity. In the present study, we explore the effect of selected linkers on the biological activity of the dimer. The linkers were designed as five-atom chains with carbon, nitrogen or oxygen in their centre. In addition, the central nitrogen was modified by a benzyl group with hydroxy or methoxy substituents and one derivative possessed an extended linker length. Thirteen new dimers were subjected to cytotoxicity assay and cell cycle profiling. Dimers containing linker with benzyl moiety substituted with one or more methoxy groups and longer branched ones were found inactive, whereas other structures had comparable efficacy as the original ED (e.g. D1 with IC_{50} = 1.53 μM). Cell cycle analysis and immunofluorescence proved the interference of dimers with microtubule assembly and mitosis. The proposed *in silico* model and calculated binding free energy by the MM-PBSA method were closely correlated with *in vitro* tubulin assembly assay.

1. Introduction

Steroids are an important group of lipophilic biologically active substances. They play several key roles in the biological environment, in particular, they are components of biological membranes or act as signalling molecules. Any change in the chemical structure of steroids can lead to change or loss of efficacy, enhancement or alteration of the mechanism of action. Chemical modifications of steroids are a popular discipline of medical chemists dealing with the discovery of new potential drugs or their transport to the target tissue.

Steroid dimers are a group of substances containing two steroid skeletons in a molecule. Such structures can also be found in nature, but most of them come from a chemical laboratory [1–3] (reviewed by Nahar et al. [4]). In our recent work, we have described the preparation and biological properties of the estradiol homodimer (**ED**, Fig. 1) linked *via* a heterocyclic bridge at the C-17 position [5]. **ED** was prepared by a CuAAC [6] reaction of 17α-ethinylestradiol (**EE**) and a heterocyclic diazide [1]. In this work, we described the cytotoxic properties and investigated the mechanism of **ED** action.

Cell cycle studies have shown an increase in cells in the G_2/M phase and polyploid cells accompanied by a decrease in DNA/RNA synthesis in CCRF-CEM cells. Further experimental work led to the conclusion that **ED** acts at the cytoskeletal level by inhibiting tubulin polymerization. **ED** has been shown to be more effective compared to the well-studied steroidal microtubule polymerization inhibitor 2-methoxyestradiol (**ME**, Fig. 1) and equipotent to nocodazole (**Noc**). Both **ED** and **Noc** completely and reversibly depolymerized microtubules in U2OS cells. Although several dimeric structures containing estradiol in the molecule can be found in the literature [7–11] (Supplementary Figure S1, compounds **s1**-**s8**) only dimer **s8** based on **ME** published by Cushman et al. [11] has shown significant activity at the cytoskeletal level. Thus, the structural motif of **ED** was found as a new type of steroid-based inhibitor of microtubule polymerization and dynamics.

In the current work, we focused on the study of dimeric structures of estradiol with a variable connecting bridge. The length of the bridge contained in twelve cases 5 atoms (**L1**-**L12**, Fig. 2) and one PEG_3 (**L13**,

* Corresponding author.
E-mail address: petr.dzubak@upol.cz (P. Džubák).

https://doi.org/10.1016/j.bioorg.2022.106334
Received 27 September 2022; Received in revised form 9 December 2022; Accepted 19 December 2022
Available online 23 December 2022
0045-2068/© 2022 The Authors. Published by Elsevier Inc. This is an open access article under the CC BY license (http://creativecommons.org/licenses/by/4.0/).

Fig. 2) linker was used. This five-atom length was derived from the structure of **ED**. The new dimers (**D1**-**D12**, Fig. 3) contained atoms such as carbon, nitrogen or oxygen in the centre of the linker. Other structures were modified with hydroxy or methoxy-substituted benzyl pendant on the central nitrogen atom in the linker. The implementation of such substituted benzyls was motivated by the structure of natural and synthetic mitotic poisons containing precisely these groups in the molecule (reviewed by Škubník et al. [12]).

2. Results and discussion

2.1. Chemistry

The design of the new estradiol dimers was inspired by results recently published by our group [5]. A new series of steroid dimers were prepared by CuAAC from diazide linkers **L1**-**L12** and **EE**. The preparation of azide-terminated bridges (**L1**-**L12**) was performed by nucleophilic substitution of corresponding alkyl halides by sodium azide in DMF at elevated temperatures (**L1**-**L3**, Fig. 2). The *N*-benzyl substituted linkers were prepared by reductive amination from the linker **L3** and variously substituted benzaldehyde derivatives containing hydroxy, methoxy or a combination of such groups. Sodium cyanoborohydride in the presence of acetic acid was used as a reducing agent (Fig. 2). These tertiary amine diazides were isolated in rather moderate yields (Fig. 2).

Estradiol dimers **D1**-**D12** were prepared *via* CuAAC from diazides **L1**-**L12** and **EE** by microwave-assisted synthesis (MW) using an optimized catalyst system operating on the principle of *in situ* reduction of Cu(II) to Cu(I) by sodium ascorbate (Fig. 3). The dimers were prepared without problems and the substances were isolated in good to excellent yields (61–94 %). Images of NMR and HRMS spectra and results from HPLC analyzes of dimers are documented as Supplementary material (Figures S2-S53).

2.2. Cytotoxicity

The prepared estradiol dimers **D1**-**D13** were tested for their cytotoxic activity against the cell line panel under *in vitro* conditions. Table 1 shows that compound **D1** possess significant cytotoxic activity against human cell lines derived from both leukaemias and solid tumours. The IC_{50} values were highly comparable with 2-methoxyestradiol (**ME**), nevertheless previously published **ED** was slightly more effective [5]. Dimers **D2**-**D4** and **D9**-**D10** exhibited a strong cytotoxic effect in leukaemia cell lines, however in some solid tumor-derived cell lines was observed lower cytotoxicity. Structures **D6** and **D8** showed weak cytotoxicity only against leukaemia cell lines, whereas **D5**, **D7**, **D11**, **D12** and **D13** showed no cytotoxic activity against all cell lines included in the panel at 50 μM concentration. A common feature of these inactive dimers is the presence of one, two or three methoxy groups at the *N*-benzyl aromatic ring. Interestingly, when a hydroxy group was introduced to the skeleton with one methoxy group, the cytotoxic activity was restored as visible from a comparison of **D5** and **D10** or **D6** and **D9**. Extension of the bridge as in the case of **D13** led to a loss of cytotoxic activity.

To monitor cytotoxicity in non-malignant cells, the panel involved cell lines MRC-5 and BJ derived from normal lung or foreskin tissue. MRC-5 cells displayed generally low sensitivity except for **D2**, **D9** and **D10**, whereas the BJ cell line was not sensitive toward the compounds. Compound **D1** exerted medium cytotoxic effect in both non-malignant cell lines. To assess the influence of drug-efflux transporters on the activity of compounds, we exploited sublines expressing proteins associated with multi-drug resistance. CEM-DNR subline overexpressing P-glycoprotein and LRP was resistant to all tested compounds in comparison with parental cell line CCRF-CEM. The IC_{50} values determined in the K562-TAX cell line expressing P-glycoprotein were also above 50 μM except for structure **D1**. **D1** displayed comparable cytotoxicity against subline K562-TAX and parental cell line K562 and the overall results suggest that it can be a substrate of LRP but not P-glycoprotein similarly to **ED** [5].

2.3. Cell cycle analysis

Cytotoxic compounds **D1**-**D4** and **D9**-**D10** were tested for their effect on CCRF-CEM proliferation and cell cycle (Fig. 4, Supplementary Table S1). Following 24-hour incubation with compounds, the cell population was examined using flow cytometry methods for DNA content and the presence of mitotic and proliferation markers. All tested compounds at high concentration induced DNA fragmentation (sub-G_1 population). The major effect of all tested compounds was mitotic arrest accompanied by the increased percentage of the polyploid cells. Treatment with compounds increased the percentage of the $pH3^{Ser10}$ positive cells as well as a fraction of cells in the G_2/M phase. In addition, all tested structures inhibited CCRF-CEM proliferation as monitored by 5-bromo-2-deoxyuridine (BrDU) incorporation into replicating DNA. A similar trend was observed by labelling with complementary marker 5-bromouridine (BrU), which reflects the rate of RNA synthesis.

2.4. Tubulin assay

We performed *in vitro* tubulin polymerization assay to examine the effect of dimers on tubulin assembly (Fig. 5). All tested active estradiol

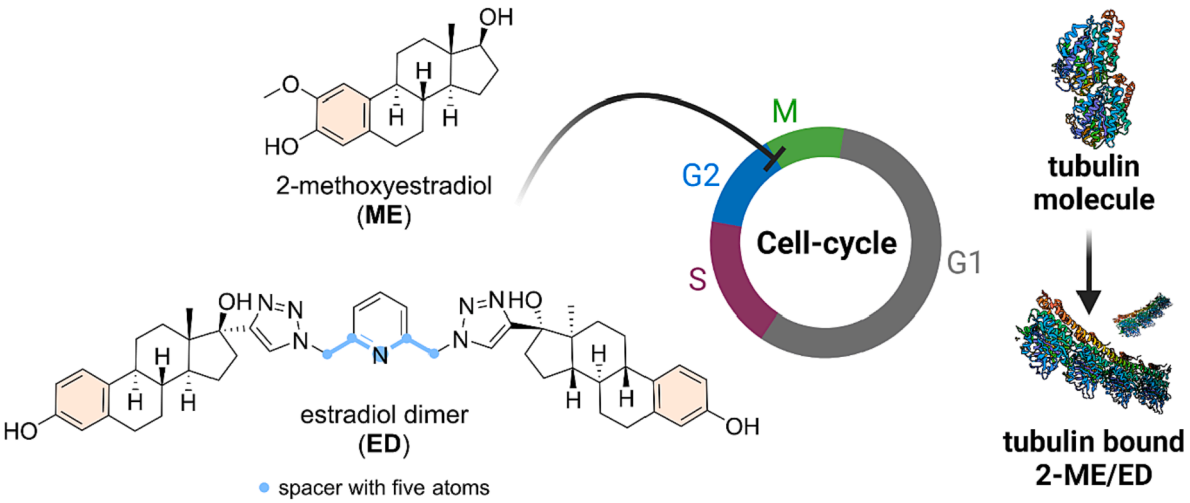

Fig. 1. Molecular structures of estradiol-based antimitotics.

dimers inhibited tubulin polymerization in comparison to the control reaction containing DMSO (Fig. 5A). The most potent compounds **D2** and **D1** flattened the polymerization curve in a similar manner as tubulin assembly inhibitor colchicine. Maximal velocity of polymerization values (V_{max}) indicates that **D2** and **D1** exerted at equimolar concentration stronger inhibition than **ED**, **ME** and nocodazole, however weaker than colchicine (Fig. 5B). Structures with *N*-benzyl aromatic ring **D3**, **D4**, **D9** and **D10** displayed comparable or better effects than nocodazole. The results suggest that **ED** activity can be improved by structural changes within the linker and simple linkers might be more suitable than the more complex ones.

2.5. Fluorescence microscopy

Immunofluorescence images revealed disruption of microtubules in U-2 OS cells following 24-hour treatment with compounds **D1**, **D2**, **D4**, **D9** and **D10** (Fig. 6; image of control is shown in Supplementary Figure S55A). All of the aforementioned substances showed an $IC_{50} < 2$ μM on U-2 OS cells (Table 1). Incubation led to complete microtubule disorganization with free unpolymerized α-tubulin in the cytoplasm. To determine whether the effect of compounds on microtubule dynamics is reversible, we observed the microtubular network after the cell washout procedure. Following the complete removal of compounds from the media the microtubular network was reestablished. Interestingly, **D3** also showed activity at the cytoskeletal level (see Supplementary Figure S55B), although its IC_{50} in U-2 OS was determined above 50 μM. The probable reason could be a differential sensitivity of leukaemia and epithelial cell lines to antimitotics. IC_{50} values of **D3** estimated for the leukaemia lines CCRF-CEM and K562 were 1.41 μM and 1.31 μM. In contrast, U2OS cell line or other epithelial cell lines such as HCT116 or A549 can for some period tolerate polyploidization and had IC_{50} values above 50 μM due to metabolization of MTS in the viability assay.

In summary, cell-based data as well as *in vitro* data demonstrate that newly developed estradiol dimers behave similarly to **ED** [5]. They inhibit tubulin polymerization, reversibly affect microtubule distribution in interphase cells and suppress microtubule dynamics effectively than **ME** or nocodazole (Fig. 5B).

2.6. In silico modelling

All compounds were docked in a tubulin structure which was complexed with colchicine (4O2B), as was demonstrated previously it fits this kind of structure better than other tubulin structures [5]. All compounds have the same binding mode. One estradiol residue is buried deep inside the colchicine binding site, whereas the other binds on the interface between α- and β-chains (Fig. 7).

We performed 150 ns molecular dynamic (MD) simulations for compounds **D1**, **D2**, **D3** and **D9**. Compounds **D1**, **D2** and **D3** have a variable effect on tubulin polymerization speed and their comparison should allow evaluation of the effect of replacement of a methylene group in the spacer with oxygen or nitrogen. Compound **D9** was chosen as one of the most active compounds in this series which has a phenylamino group within the spacer. The ligand poses found in docking did not fluctuate much in MD simulations that supported their validity (Figure S56). The majority of contacts for all ligands identified by ProLIF [13] were hydrophobic, which was expected due to the hydrophobic nature of molecules (Fig. 8, Figure S57). **D1** formed stable H-bonds with backbone carbonyl groups of Val236B and Thr179A, which were observed during the whole simulation. Both these contacts were created by two hydroxyl groups of the inner estradiol moiety. The outer estradiol was bound to the hydroxyl group of Tyr210A for most of the time, but closer to the end of the simulation the estradiol moiety was slightly shifted and the contact was broken. The spacer is surrounded by water molecules but also participates in hydrophobic contacts with suitable amino acid residues (Fig. 8A). The inner estradiol moiety of **D2** contacted with Val236B and Thr179A similar to **D1**, but the former bond was quickly broken because the moiety was shifted outside. The hydroxyl group of the outer estradiol moiety formed stable contacts with the backbone carbonyl of Gln176A and a hydroxyl group of Tyr210A. The oxygen in the spacer was not involved in H-bonding with tubulin for most of the time, occasionally forming H-bonds with a hydroxyl group of Thr178A (Fig. 8B). The hydroxyl group of the inner estradiol moiety of **D3** formed stable H-bonds with Val236B, while the hydroxyl group of the outer moiety with Gln176A. This is similar to **D1** and **D2**. The protonated amino group in the spacer created a stable H-bond with the hydroxyl group of Ser178A, which was observed for the whole simulation, and occasionally contacted with Asp327B (Fig. 8C). **D9** created several contacts stable in the course of the whole simulation – the hydroxyl group of the outer estradiol moiety formed H-bond with the hydroxyl group of Thr178A, the hydroxyl group of the 4-hydroxy-3-methoxyphenylamino group created H-bond with the hydroxyl of Tyr210A, the protonated nitrogen atom formed H-bond with the backbone carbonyl of Gln176A and an ion interaction with Asp237B (Fig. 8D). The outer estradiol moiety of **D9** was directed outside of the cavity and was not tightly bound to the protein surface, unlike the other three ligands.

The calculated binding free energy by the MM-PBSA method was in good agreement with the observed polymerization speed caused by these inhibitors, compounds with stronger inhibiting polymerization speed had lower binding free energy (Table 2).

Only the binding energy of **D1** was overestimated. We hypothesize that the observed difference in the inhibitory activity of these compounds can be explained by the entropy factor. Ligands comprising a protonated nitrogen within their flexible spacers (**D3** and **D9**) formed charged H-bonds and ionic interactions with the protein. Thus, they should lose more degrees of freedom upon binding which may result in less favourable binding entropy than in the case of compounds **D1** and **D2**. The spacer of compound **D1** does not form any specific interactions with the protein and the spacer of **D2** comprising an oxygen atom forms H-bonds occasionally, therefore movement of these ligands is less restricted. This hypothesis is indirectly confirmed by the calculated interaction entropy, which was the largest for **D3** and **D9** (Table 2).

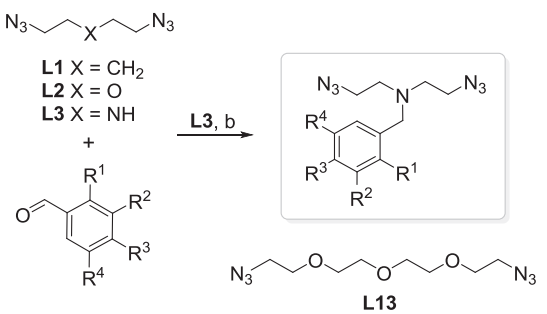

Linker	R^1	R^2	R^3	R^4	yield (%)
L4	H	H	H	H	61
L5	H	H	OMe	H	43
L6	H	OMe	H	H	58
L7	OMe	OMe	H	H	48
L8	H	OMe	OMe	H	53
L9	H	OMe	OH	H	17
L10	H	OH	OMe	H	41
L11	H	OMe	OMe	OMe	55
L12	OMe	OMe	OMe	H	42

Fig. 2. Synthesis of benzyl substituted diazides. *Reagents and conditions*: $NaCNBH_3$, HOAc, MeOH, 90 min, RT.

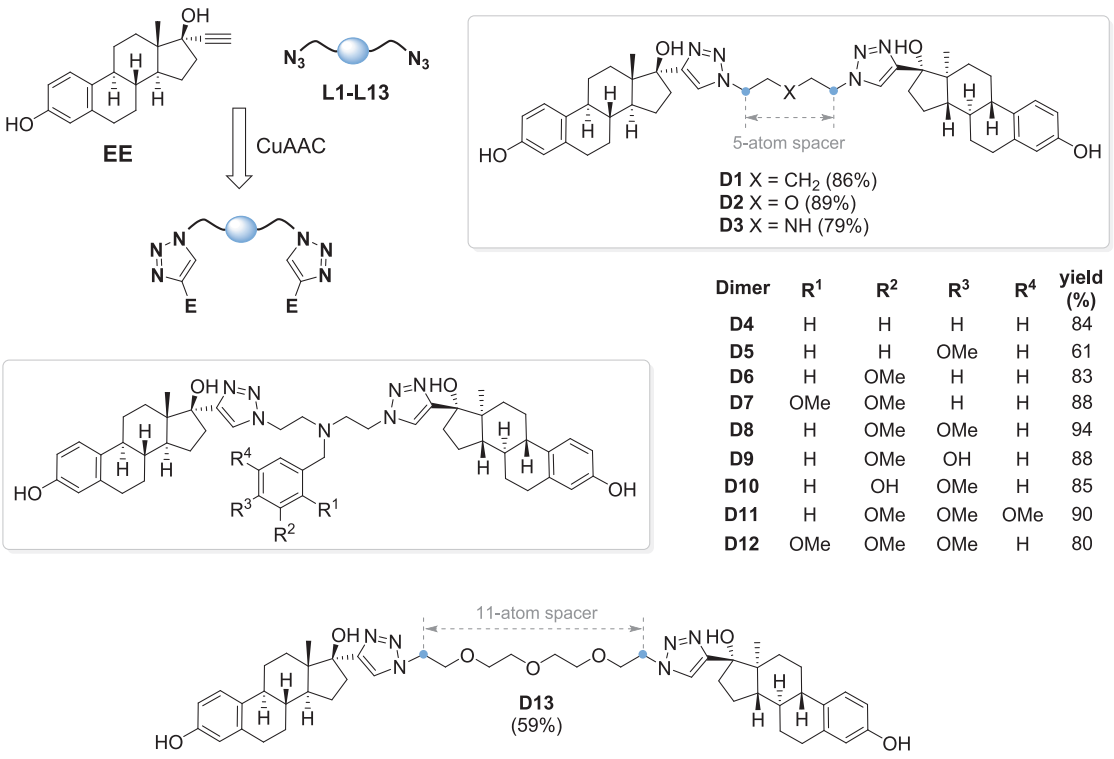

Dimer	R^1	R^2	R^3	R^4	yield (%)
D4	H	H	H	H	84
D5	H	H	OMe	H	61
D6	H	OMe	H	H	83
D7	OMe	OMe	H	H	88
D8	H	OMe	OMe	H	94
D9	H	OMe	OH	H	88
D10	H	OH	OMe	H	85
D11	H	OMe	OMe	OMe	90
D12	OMe	OMe	OMe	H	80

Fig. 3. Structures of synthesized estradiol dimers. *CuAAC:* $CuSO_4 \cdot 5H_2O$, sodium ascorbate, DMF, MW-80 °C, 2 h.

Table 1
Cytotoxic activity was determined using an MTS assay following 3-day incubation. Values represent the means of IC_{50} from 3 independent experiments with SD ranging from 10 to 25 % of the average values. [a]Tested cell lines: CCRF-CEM (childhood T acute lymphoblastic leukaemia), CEM-DNR (CCRF-CEM daunorubicin resistant), K562 (chronic myelogenous leukaemia), K562-Tax (K562 paclitaxel-resistant), A549 (lung adenocarcinoma), HCT116 (colorectal cancer), HCT116p53-/- (null p53 gene), U2OS (osteosarcoma). Normal human cell lines: MRC-5 and BJ (normal cycling fibroblasts). EE = 17α-ethinylestradiol, ME = 2-methoxyestradiol, ED = estradiol dimer [5]. Data show the average from three independent replicates and the standard deviation in cytotoxicity assays is typically up to 15 % of the average value.

Compd. Cell line[a]	EE	ME	ED	D1	D2	D3	D4	D6	D8	D9	D10
IC_{50} [μM]											
CCRF-CEM	22.58	1.55	0.48	1.53	1.49	1.43	1.21	16.04	12.08	1.22	1.39
CEM-DNR	21.79	1.67	>50	>50	>50	>50	>50	>50	>50	>50	>50
K562	8.43	1.66	0.58	1.25	1.21	1.31	1.31	12.38	9.59	1.11	1.08
K562-TAX	14.89	1.18	3.54	1.65	>50	>50	>50	>50	>50	>50	>50
A549	33.20	2.25	1.12	1.55	>50	>50	>50	>50	>50	>50	>50
HCT116	31.31	1.68	0.95	1.48	2.12	>50	2.50	>50	>50	1.71	1.70
HCT116p53-/-	29.88	1.79	0.90	1.45	1.83	>50	2.26	>50	>50	1.60	1.70
U2OS	22.77	1.98	6.28	1.96	3.04	>50	1.96	>50	>50	7.35	2.68
MRC-5	>50	>50	1.15	30.32	3.00	>50	>50	>50	>50	10.64	2.76
BJ	>50	>50	>50	13.91	>50	>50	>50	>50	>50	>50	>50

3. Conclusions

On the newly synthesized thirteen estradiol dimers (**D1**-**D13**), we have shown that structural changes in the bridge are very important for the activity of estradiol dimers at the cytoskeletal level. Introduction of a bulky group into the linker (benzyl pendants) usually reduces the activity of dimers. Likewise, extending the bridge leads to a loss of activity (**D13**). We have confirmed that all of the active dimers behave similarly to **ED** by reversible inhibition of tubulin polymerization which is favorable, and in such cases, less toxicity, compared to irreversible inhibitor colchicine, is expected in the therapeutical use in humans [14]. The results indicate that the activity of the originally discovered **ED** [5] can be further modulated by structural changes in the linker, and for targeting tubulin, simple linkers seem more suitable than more complex ones.

4. Experimental

4.1. Chemistry

4.1.1. General methods and materials

For thin-layer chromatography (TLC), aluminium silica gel sheets for detection in UV light (TLC silica gel 60 F254, Merck) were used. For TLC visualization, a diluted solution of H_2SO_4 in MeOH was used and plates were heated. For column chromatography, 30–60 μm silica gel (ICN Biomedicals, Costa Mesa, USA) was used. NMR spectra were recorded by Agilent-MR DDR2 and Varian Gemini 300 (Varian, Palo Alto, CA, USA). The Quadrupole LC/MS (ESI ionization) with an Infinity III LC system (Agilent Technologies, Santa Clara, USA) was used for LR-MS and HPLC analyses (C18 column: 100 mm; UV detection). The method for HPLC was as follows (A – 50 % MeOH, B – 100 % MeOH): 0 min 100 % A; 2 min 100 % B; 2 – 16 min 100 %; 18 min 50 % A; 20 min 100 % A. HRMS

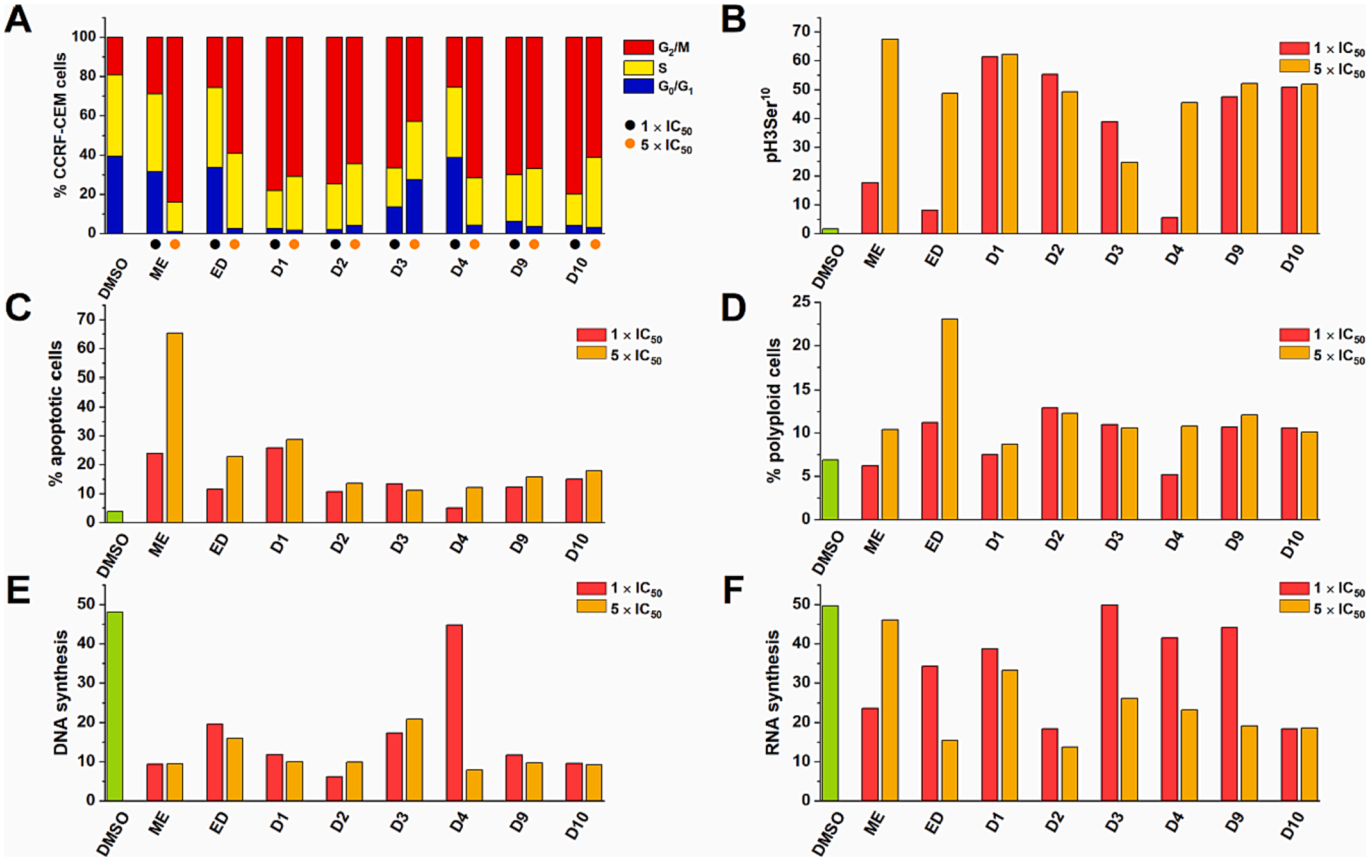

Fig. 4. Effect of cytotoxic compounds on the cell cycle (A), mitosis (B), apoptosis (C), induction of polyploidy (D) and DNA/RNA synthesis (E, F, resp.) in CCRF-CEM lymphoblasts (% of positive cells). Flow cytometry analysis was used for the quantification of cell cycle distribution and apoptotic cells with a concentration of compounds equal to 1 × IC_{50} and 5 × IC_{50} values. The DNA fragmentation was assessed using the logarithmic model expressing the percentage of the particles with the propidium iodide content lower than cells in the G_0/G_1 phase (<G_1) of the cell cycle. The table with values is available in Suppl. Mat. as Table S1 and raw data are depicted in Figure S54.

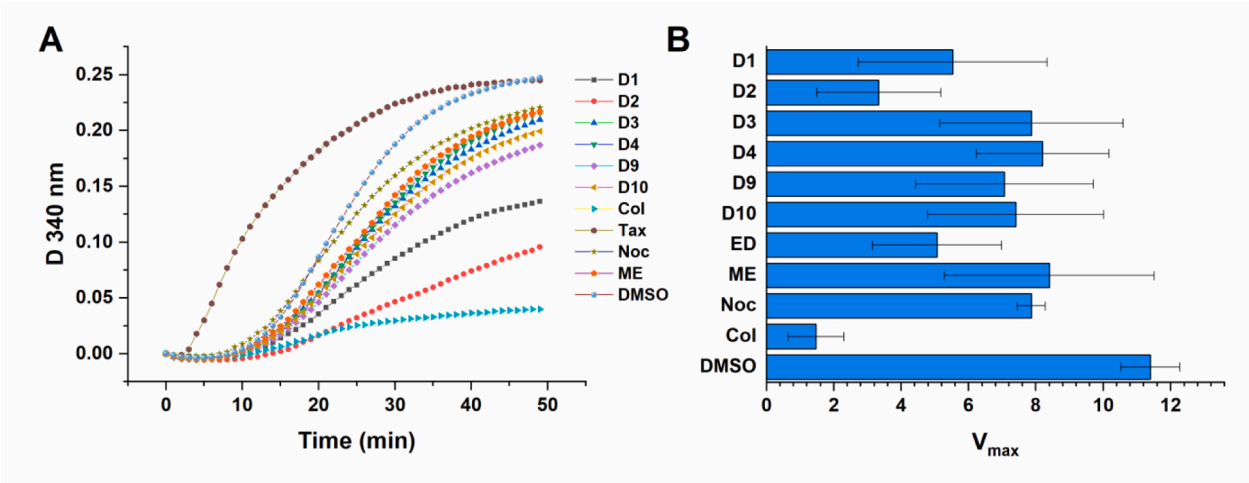

Fig. 5. Inhibition of tubulin assembly by dimers in a turbidometric tubulin polymerization assay (A). 10 μmol/L of dimers D1, D2, D3, D4, D9, D10, 2-methoxyestradiol (ME), taxol (Tax), nocodazole (Noc), colchicine (Col) or corresponding volume of DMSO were used. Polymerization curves are mean values from three independent experiments. The maximal velocity of polymerization values (V_{max}) was calculated from tubulin polymerization curves in the growth phase (B).

spectra were measured by Micro Q-TOF with ESI ionization (Thermo Scientific, Waltham, USA). Optical rotations were measured with an Autopol VI polarimeter (Rudolph Research Analytical, Hackettstown, NJ, USA). For microwave synthesis (MW), an Initiator Classic 355,301 (Biotage, Uppsala, Sweden) was used. Chemicals were purchased from TCI Europe (Zwijndrecht, Belgium): sodium ascorbate (>99 %), ethinylestradiol – EE (>98 %); and from Sigma-Aldrich (St. Louis, MO, USA): copper(II) sulfate pentahydrate – $CuSO_4 \cdot 5H_2O$ (≥98 %), benzaldehyde (≥99 %), 4-methoxybenzaldehyde (98 %), 3-methoxybenzaldehyde (97 %), 2,3- dimethoxybenzaldehyde (98 %), 3,4-

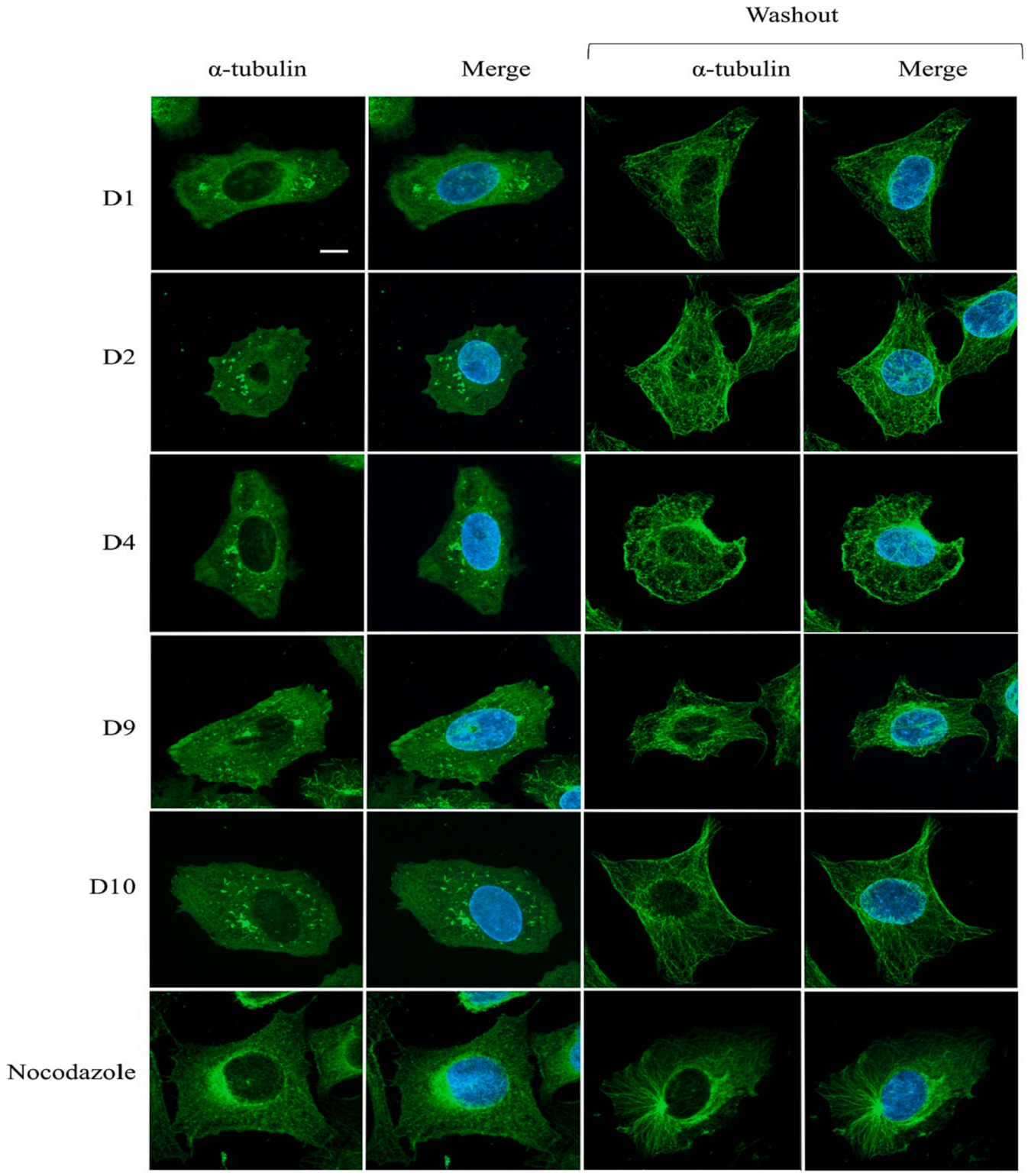

Fig. 6. Immunofluorescent images of U2OS cells treated for 24 h with 10 μM concentration of dimers or 0.75 μM nocodazole. For the purpose of the washout experiment the media with compounds were aspirated, coverslips with cells washed 3 times and incubated for an additional 30 min in the incubator in cultivation media. Nuclei were stained using Hoechst 33,342 (blue) and α-tubulin with primary antibody and secondary Alexa Fluor 488-conjugated antibody (green). Scale bar 10 μm. (For interpretation of the references to colour in this figure legend, the reader is referred to the web version of this article.)

dimethoxybenzaldehyde (99 %), vanillin (99 %), isovanillin (99 %), 3,4,5-trimethoxybenzaldehyde (98 %), 2,3,4-trimethoxybenzaldehyde (99 %), 1,11-diazido-3,6,9-trioxaundecane (**L13**). Solvents for column chromatography and reactions supplied by PENTA (Praha, Czech Republic) were used as delivered. Synthesis of some diazides was previously described, namely: 1,5-diazidopentane (**L1**) [15], bis(2-azidoethyl)ether (**L2**) [15] and *N,N*-bis(2-azidoethyl)amine (**L3**) [16].

4.1.2. Synthesis of diazides

General procedure: To **L3** (250 mg, 1.61 mmol, 1 equiv.) and

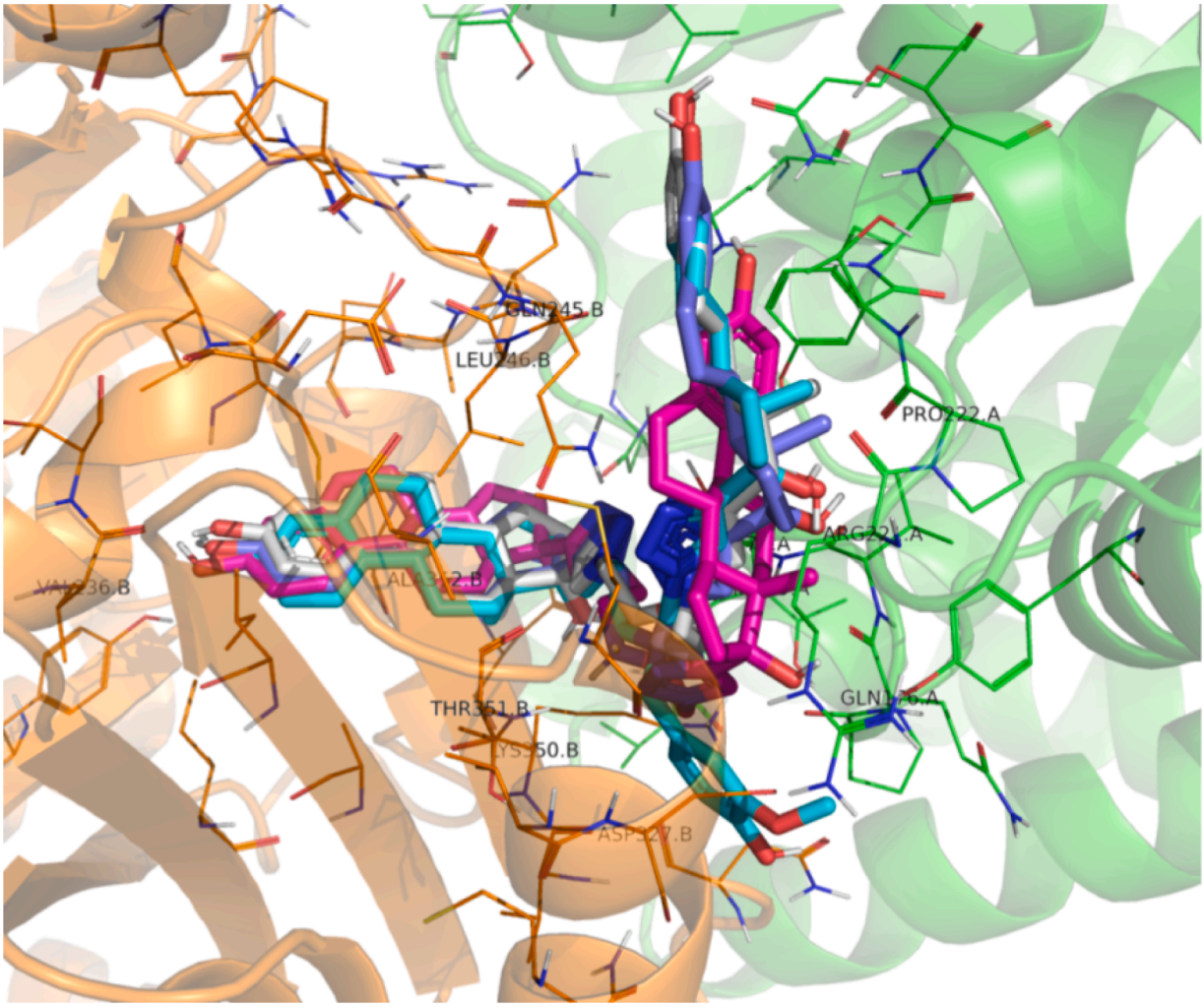

Fig. 7. Docking poses of compounds D1 (blue), D2 (grey), D3 (magenta) and D9 (cyan). (For interpretation of the references to colour in this figure legend, the reader is referred to the web version of this article.)

aldehyde (1 equiv.) in MeOH (15 mL) HOAc (193 mg, 3.2 mmol, 2 equiv.) and $NaCNBH_3$ (202 mg, 3.2 mmol, 2 equiv.) were added at RT. The mixture was stirred for 90 min after which the solvents were evaporated under reduced pressure. Chloroform (25 mL) was added and the solids were filtered off. The solvent was evaporated and the crude product was purified by silica gel column chromatography.

2-Azido-*N*-(2-azidoethyl)-*N*-benzylethan-1-amine (**L4**).

Reaction with benzaldehyde (171 mg, 1.61 mmol). Chromatography using hexanes-AcOEt 5:1 (*v*/*v*). **L4** (240 mg, 0.98 mmol) was isolated as a slightly yellowish oil in 61 % yield. $\mathbf{R_F}$ = 0.8 in hexanes-AcOEt 5:1 (*v*/*v*). **^{1}H NMR** (300 MHz, $CDCl_3$) δ ppm: 2.78 (t, *J* = 6.1 Hz, 4H), 3.31 (t, *J* = 6.1 Hz, 4H), 3.73 (s, 2H), 7.26–7.33 (m, 1H), 7.34–7.45 (m, 4H). **^{13}C NMR** (75 MHz, $CDCl_3$) δ ppm: 49.45, 53.68, 59.34, 127.40, 128.50, 128.76, 138.59. **LRMS-ESI**: calcd 245.1 Da, found *m*/*z* 246.2 $[M + H]^+$.

2-Azido-*N*-(2-azidoethyl)-*N*-(4-methoxybenzyl)ethan-1-amine (**L5**).

Reaction with 4-methoxybenzaldehyde (219 mg, 1.61 mmol). Chromatography using hexanes-AcOEt 4:1 (*v*/*v*). **L5** (190 mg, 0.69 mmol) was isolated as a colorless oil in 43 % yield. $\mathbf{R_F}$ = 0.7 in hexanes-AcOEt 4:1 (*v*/*v*). **^{1}H NMR** (300 MHz, $CDCl_3$) δ ppm: 2.74 (t, *J* = 6.2 Hz, 4H), 3.28 (t, *J* = 6.2 Hz, 4H), 3.64 (s, 2H), 3.80 (s, 3H), 6.84–6.91 (m, 2H), 7.23–7.30 (m, 2H). **^{13}C NMR** (75 MHz, $CDCl_3$) δ ppm: 49.43, 53.54, 55.22, 58.68, 113.81, 129.90, 130.44, 158.91. **LRMS-ESI**: calcd 275.1 Da, found *m*/*z* 276.2 $[M + H]^+$.

2-Azido-*N*-(2-azidoethyl)-*N*-(3-methoxybenzyl)ethan-1-amine (**L6**).

Reaction with 3-methoxybenzaldehyde (219 mg, 1.61 mmol). Chromatography using hexanes-AcOEt 4:1 (*v*/*v*). **L6** (260 mg, 0.94 mmol) was isolated as an yellowish oil in 58 % yield. $\mathbf{R_F}$ = 0.8 in hexanes-AcOEt 4:1 (*v*/*v*).**^{1}H NMR** (300 MHz, $CDCl_3$) δ ppm: 2.76 (t, *J* = 5.9 Hz, 4H), 3.30 (t, *J* = 5.9 Hz, 4H), 3.68 (s, 2H), 3.81 (s, 3H), 6.83 (dd, *J* = 7.9, 2.1 Hz, 1H), 6.92 (d, *J* = 7.0 Hz, 1H), 6.97–7.02 (m, 1H), 7.20–7.28 (m, 1H). **^{13}C NMR** (75 MHz, $CDCl_3$) δ ppm: 49.40, 53.75, 55.16, 59.31, 113.28, 113.64, 120.90, 129.37, 140.32, 159.87. **LRMS-ESI**: calcd 275.2 Da, found *m*/*z* 276.2 $[M + H]^+$.

2-Azido-*N*-(2-azidoethyl)-*N*-(2,3-dimethoxybenzyl)ethan-1-amine (**L7**).

Reaction with 2,3-dimethoxybenzaldehyde (268 mg, 1.61 mmol). Chromatography using hexanes-AcOEt 4:1 (*v*/*v*). **L7** (239 mg, 0.78 mmol) was obtained as a slightly yellowish oil in 48 % yield. $\mathbf{R_F}$ = 0.7 in hexanes-AcOEt 3:1 (*v*/*v*). **^{1}H NMR** (300 MHz, $CDCl_3$) δ ppm: 2.74 (t, *J* = 6.2 Hz, 4H), 3.30 (t, *J* = 6.4 Hz, 4H), 3.73 (s, 2H), 3.81 (s, 3H), 3.84 (s, 3H), 6.83 (dd, *J* = 7.3, 2.6 Hz, 1H), 6.97–7.07 (m, 2H).**^{13}C NMR** (75 MHz, $CDCl_3$) δ ppm: 49.45, 52.30, 53.52, 55.66, 60.71, 111.35, 122.18, 123.93, 131.87, 147.54, 152.68. **LRMS-ESI**: calcd 305.2 Da, found *m*/*z* 306.2 $[M + H]^+$.

2-Azido-*N*-(2-azidoethyl)-*N*-(3,4-dimethoxybenzyl)ethan-1-amine (**L8**).

Reaction with 3,4-dimethoxybenzaldehyde (268 mg, 1.61 mmol). Chromatography using hexanes-AcOEt 4:1 (*v*/*v*). **L8** (263 mg, 0.86 mmol) was obtained as a slightly colorless oil in 53 % yield. $\mathbf{R_F}$ = 0.6 in hexanes-AcOEt 3:1 (*v*/*v*). **^{1}H NMR** (300 MHz, $CDCl_3$) δ ppm: 2.68 (t, *J* =

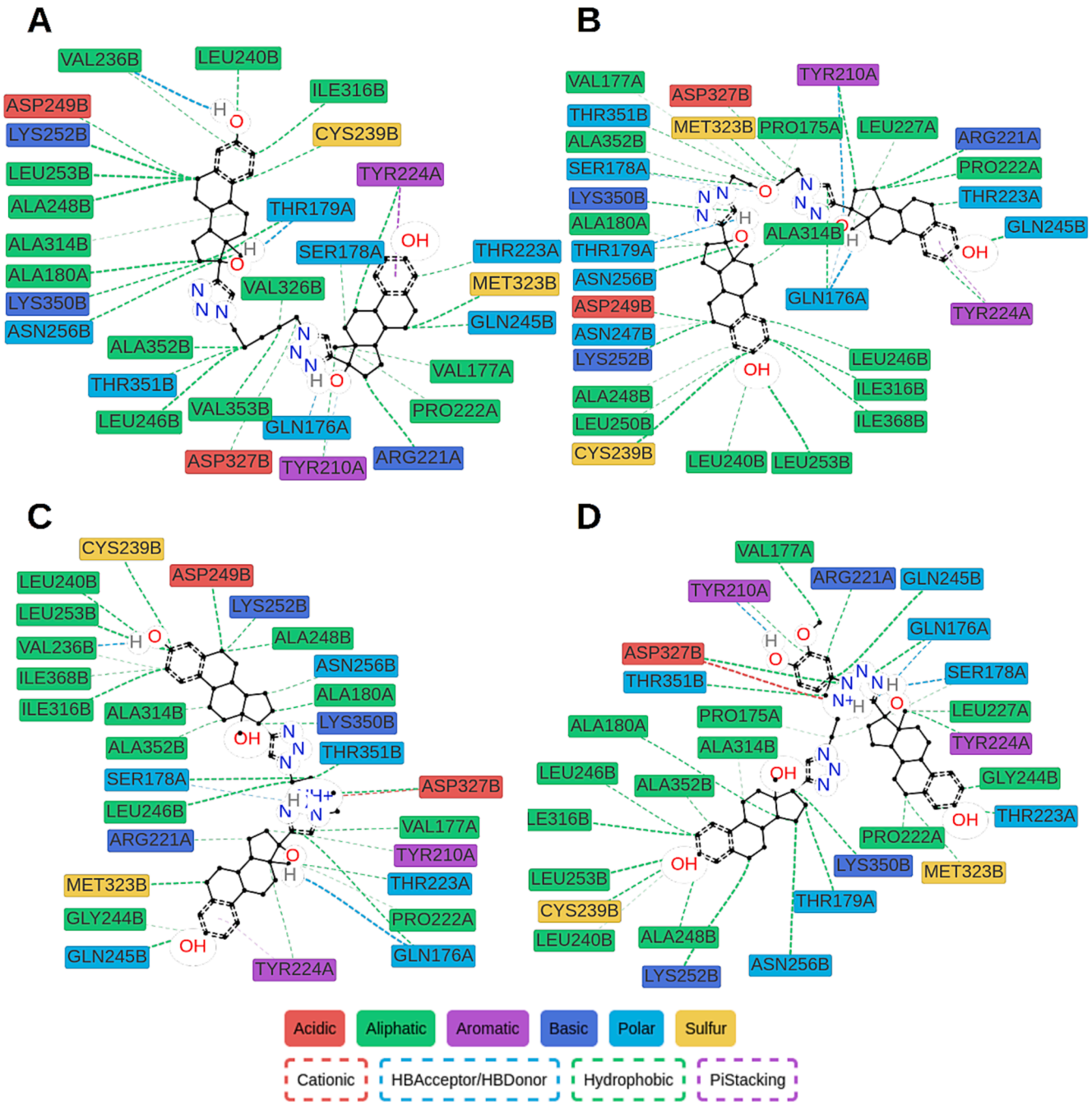

Fig. 8. Protein-ligand contacts were observed in at least 10 % of MD trajectories for D1 (A), D2 (B), D3 (C) and D9 (D). Contacts were analyzed only for the stable part of trajectories, 50–150 ns.

Table 2
Calculated binding free energy by MM-PBSA method, interaction entropy and maximal velocity of polymerization.

Dimer	ΔG [kcal·mol^{-1}]	-TΔS [kcal·mol^{-1}]	Vmax
D1	−22.6	16.8	4.1
D2	−19.4	13.0	2.8
D3	−2.9	28.8	7.4
D9	−5.6	35.6*	5.9

*Calculated interaction entropy for compound **D9** had a large standard deviation (6.5) whereas for other ligands it did not exceed 0.05.

5.9 Hz, 4H), 3.22 (t, J = 6.2 Hz, 4H), 3.57 (s, 2H), 3.80 (s, 3H), 3.82 (s, 3H), 6.70–6.81 (m, 2H), 6.95 (s, 1H). **^{13}C NMR** (75 MHz, $CDCl_3$) δ ppm: 49.31, 53.72, 55.74, 55.80, 59.13, 110.68, 111.48, 120.64, 131.13, 148.22, 149.11. **LRMS-ESI**: calcd 305.2 Da, found m/z 306.2 $[M + H]^+$.

4-((Bis(2-azidoethyl)amino)methyl)-2-methoxyphenol (**L9**).

Reaction with vanillin (245 mg, 1.61 mmol). Chromatography using hexanes-AcOEt 4:1 (v/v). **L9** (78 mg, 0.27 mmol) was obtained as an oil in 17 % yield. **R_F** = 0.7 in hexanes-AcOEt 3:1 (v/v). **^{1}H NMR** (300 MHz, $CDCl_3$) δ ppm: 2.76 (t, J = 5.9 Hz, 4H), 3.30 (t, J = 5.9 Hz, 4H), 3.62 (s, 2H), 3.89 (s, 3H), 5.73 (br. s., 1H), 6.73–6.79 (m, 1H), 6.83–6.88 (m, 1H), 7.01 (s, 1H). **^{13}C NMR** (75 MHz, $CDCl_3$) δ ppm: 49.37, 53.74, 55.90, 59.29, 110.96, 113.89, 121.38, 130.47, 144.90, 146.83. **LRMS-ESI**: calcd 291.1 Da, found m/z 292.1 $[M + H]^+$.

5-((Bis(2-azidoethyl)amino)methyl)-2-methoxyphenol (**L10**).

Reaction with isovanillin (245 mg, 1.61 mmol). Chromatography using hexanes-AcOEt 4:1 (*v/v*). **L10** (191 mg, 0.66 mmol) was obtained as an oil in 41 % yield. $\mathbf{R_F}$ = 0.6 in hexanes-AcOEt 3:1 (*v/v*). **^{1}H NMR** (300 MHz, $CDCl_3$) δ ppm: 2.73 (t, *J* = 5.9 Hz, 4H), 3.28 (t, *J* = 5.9 Hz, 4H), 3.59 (s, 2H), 3.86 (s, 3H), 5.84 (br. s., 1H), 6.77–6.84 (m, 2H), 6.87–6.93 (m, 1H). **^{13}C NMR** (75 MHz, $CDCl_3$) δ ppm: 49.42, 53.49, 55.98, 58.76, 110.59, 115.05, 120.27, 131.63, 145.57, 145.92. **LRMS-ESI**: calcd 291.1 Da, found *m/z* 292.2 $[M + H]^+$.

2-Azido-*N*-(2-azidoethyl)-*N*-(3,4,5-trimethoxybenzyl)ethanamine (**L11**).

Reaction with 3,4,5-trimethoxybenzaldehyde (316 mg, 1.61 mmol). Chromatography using hexanes-AcOEt 2:1 (*v/v*). **L11** (298 mg, 0.89 mmol) was obtained as a colorless gel in 55 % yield. $\mathbf{R_F}$ = 0.7 in hexanes-AcOEt 2:1 (*v/v*). **^{1}H NMR** (400 MHz, $CDCl_3$) δ ppm: 2.75 (t, *J* = 6.1 Hz, 4H), 3.30 (t, *J* = 5.9 Hz, 4H), 3.63 (s, 2H), 3.83 (s, 3H), 3.84 (s, 6H), 6.61 (s, 2H). **^{13}C NMR** (101 MHz, $CDCl_3$) δ ppm: 49.34, 53.83, 56.03, 59.67, 60.82, 105.05, 134.37, 136.91, 153.23. **LRMS-ESI**: calcd 335.2 Da, found *m/z* 336.2 $[M + H]^+$.

2-Azido-*N*-(2-azidoethyl)-*N*-(2,3,4-trimethoxybenzyl)ethanamine (**L12**).

Reaction with 2,3,4-trimethoxybenzaldehyde (316 mg, 1.61 mmol). Chromatography using hexanes-AcOEt 3:1 (*v/v*). **L12** (226 mg, 0.67 mmol) was obtained as a colorless gel in 42 % yield. $\mathbf{R_F}$ = 0.7 in hexanes-AcOEt 2:1 (*v/v*). **^{1}H NMR** (400 MHz, $CDCl_3$) δ ppm: 2.74 (t, *J* = 6.3 Hz, 4H), 3.31 (t, *J* = 6.3 Hz, 4H), 3.65 (s, 2H), 3.85 (s, 3H), 3.86 (s, 3H), 3.88 (s, 3H), 6.66 (d, *J* = 8.6 Hz, 1H), 7.04 (d, *J* = 8.6 Hz, 1H). **^{13}C NMR** (101 MHz, $CDCl_3$) δ ppm: 49.42, 52.50, 53.41, 55.93, 60.75, 61.02, 107.14, 123.84, 124.71, 142.12, 152.31, 153.03. **LRMS-ESI**: calcd 335.2 Da, found *m/z* 336.2 $[M + H]^+$.

4.1.3. Synthesis of dimers

General procedure: To a solution of diazide (**L1**-**L13**, 1 equiv.) and 17α-ethinylestradiol (**EE**, 2.2 equiv.) in dry DMF aqueous solutions (250 μL) of $CuSO_4{\cdot}5H_2O$ (0.1 equiv.) and sodium ascorbate (0.15 equiv.) were added. The mixture was placed in a microwave reactor and heated to 80 °C for 2 h. Solvents were evaporated under reduced pressure and the crude product was purified by column chromatography on silica gel. The product thus obtained was precipitated, filtered, washed with ether and dried *in vacuo*.

(17β,17′β)-17,17′-[Pentane-1,5-diylbis(1*H*-1,2,3-triazole-1,4-diyl)] bisestra-1,3,5(10)-triene-3,17-diol (**D1**).

In reaction: **L1** (50 mg, 0.32 mmol), **EE** (210 mg, 0.71 mmol), $CuSO_4{\cdot}5H_2O$ (18 mg, 0.071 mmol), sodium ascorbate (21 mg, 0.1 mmol), DMF (6 mL). Chromatography with $CHCl_3$-MeOH 20:1 → 10:1 → 5:1 (*v/v*). Compound **D1** (209 mg, 0.28 mmol) was obtained as a white solid in 86 % yield. $\mathbf{R_F}$ = 0.2 in DCM-MeOH 10:1 (*v/v*). **^{1}H NMR** (400 MHz, DMSO-d_6) δ ppm: 0.58 (td, *J* = 12.7, 3.1 Hz, 2H), 0.92 (s, 6 H), 1.13–1.53 (m, 12H), 1.58–1.69 (m, 2 H), 1.72–2.00 (m, 11*H*), 2.04–2.15 (m, 2 H), 2.28–2.43 (m, 2 H), 2.63–2.78 (m, 4 H), 4.31 (t, *J* = 7 Hz, 4 H), 5.08 (s, 2 H), 6.41 (d, *J* = 2.4 Hz, 2 H), 6.46 (dd, *J* = 8.6, 2.4 Hz, 2 H), 6.96 (d, *J* = 8.6 Hz, 2 H), 7.84 (s, 2 H), 8.96 (s, 2 H); Fig. S2.13C **NMR** (101 MHz, DMSO-d_6) δ ppm: 14.83, 23.29, 24.01, 26.52, 27.64, 29.54, 29.72, 33.12, 37.66, 43.63, 47.12, 47.95, 49.32, 81.52, 113.08, 115.31, 122.94, 126.45, 130.85, 137.59, 154.51, 155.30; Fig. S3. **HRMS-ESI**: (calcd 746.45195 Da), found *m/z* 769.44140 $[M + Na]^+$; Fig. S4. $[\alpha]_D^{20}$=+60.8 (*c* = 0.25, DMF-$CHCl_3$, 1:1). **HPLC**: R_T = 7.425 min; Fig. S5.

17,17′-{Oxybis[(ethane-2,1-diyl)-1*H*-1,2,3-triazole-1,4-diyl]}di [estra-1,3,5(10)-triene-3,17β-diol] (**D2**).

In reaction: **L2** (50 mg, 0.32 mmol), **EE** (210 mg, 0.71 mmol), $CuSO_4{\cdot}5H_2O$ (18 mg, 0.071 mmol), sodium ascorbate (21 mg, 0.1 mmol), DMF (6 mL). Chromatography with DCM-MeOH 15:1 → 10:1 → 5:1 (*v/v*). Compound **D2** (217 mg, 0.29 mmol) was obtained as a white solid in 89 % yield. $\mathbf{R_F}$ = 0.2 in DCM-MeOH 10:1 (*v/v*). **^{1}H NMR** (400 MHz, DMSO-d_6) δ ppm: 0.58 (td, *J* = 12.7, 3.5 Hz, 2H), 0.92 (s, 6H), 1.12–1.52 (m, 10*H*), 1.54–1.69 (m, 2H), 1.70–1.88 (m, 6H), 1.89–2.00 (m, 2H), 2.01–2.14 (m, 2H), 2.31–2.43 (m, 2H) 2.60–2.78 (m, 4H), 3.81 (t, *J* = 5.5 Hz, 4H), 4.48 (td, *J* = 5.3, 2.0 Hz, 4H), 5.12 (s, 2H), 6.40 (d, 2H), 6.45 (dd, *J* = 8.4, 2.5 Hz, 2H), 6.95 (d, *J* = 8.2 Hz, 2H), 7.81 (s, 2H), 8.95 (s, 2H); Fig. S6. **^{13}C NMR** (101 MHz, DMSO-d_6) δ ppm: 14.83, 24.02, 26.52, 27.64, 29.71, 33.08, 37.58, 43.62, 47.14, 47.96, 49.49, 69.13, 81.54, 113.07, 115.30, 120.41, 123.46, 126.45, 130.86, 137.59, 154.48, 155.30; Fig. S7. **HRMS-ESI**: calcd 748.43122 Da, found *m/z* 749.43843 $[M + H]^+$, 771.42062 $[M + Na]^+$ and 787.39343 $[M + K]^+$; Fig. S8. $[\alpha]_D^{28}$ = +70.4 (*c* = 0.25, DMF-$CHCl_3$, 1:1). **HPLC**: R_T = 7.573 min; Fig. S9.

(17β,17′β)-17,17′-[Iminobis(ethane-2,1-diyl-1*H*-1,2,3-triazole-1,4-diyl)]bisestra-1,3,5(10)-triene-3,17-diol (**D3**).

In reaction: **L3** (50 mg, 0.32 mmol), **EE** (210 mg, 0.71 mmol), $CuSO_4{\cdot}5H_2O$ (18 mg, 0.071 mmol), sodium ascorbate (21 mg, 0.1 mmol), DMF (6 mL). Chromatography with $CHCl_3$-MeOH 10:1 (*v/v*). Compound **D3** (189 mg, 0.25 mmol) was obtained as a white solid in 79 % yield. $\mathbf{R_F}$ = 0.15 in DCM-MeOH 10:1 (*v/v*). **^{1}H NMR** (400 MHz, DMSO-d_6) δ ppm: 0.60 (td, *J* = 12.8, 3.7 Hz, 2H), 0.92 (s, 6H), 1.12–1.52 (m, 10*H*), 1.58–2.15 (m, 13H), 2.30–2.40 (m, 2H), 2.61–2.77 (m, 4H), 2.97 (br t, *J* = 6.5 Hz, 4H), 4.35 (t, *J* = 6.5 Hz, 3 H), 5.08 (s, 2H), 6.41 (d, *J* = 2.4 Hz, 2H), 6.46 (dd, *J* = 8.4, 2.5 Hz, 2H), 6.95 (d, *J* = 8.6 Hz, 2H), 7.80–7.91 (s, 2H), 8.88–9.01 (s, 2H); Fig. S10. **^{13}C NMR** (101 MHz, DMSO-d_6) δ ppm: 14.8, 24.0, 26.5, 27.6, 29.7, 33.1, 37.6, 43.6, 47.1, 47.9, 48.8, 49.8, 81.6, 113.1, 115.3, 123.4, 126.4, 130.9, 137.6, 154.3, 155.3; Fig. S11. **HRMS-ESI**: calcd 747.44720 Da, found *m/z* 748.45435 $[M + H]^+$, 770.43622 $[M + Na]^+$ and 786.40954 $[M + K]^+$; Fig. S12. $[\alpha]_D^{28}$ = +66.5 (*c* = 0.26, DMF-$CHCl_3$, 1:1). **HPLC**: R_T = 7.587 min; Fig. S13.

17β,17′β)-17,17′-[(Benzylimino)bis(ethane-2,1-diyl-1*H*-1,2,3-triazole-1,4-diyl)]bisestra-1,3,5(10)-triene-3,17-diol (**D4**).

In reaction: **L4** (100 mg, 0.41 mmol), **EE** (266 mg, 0.9 mmol), $CuSO_4{\cdot}5H_2O$ (22 mg, 0.09 mmol), sodium ascorbate (27 mg, 0.14 mmol), DMF (8 mL). Chromatography with DCM-MeOH 10:1 (*v/v*). Compound **D4** (287 mg, 0.34 mmol) was obtained as a white solid in 84 % yield. $\mathbf{R_F}$ = 0.2 in DCM-MeOH 10:1 (*v/v*). **^{1}H NMR** (400 MHz, DMSO-d_6) δ ppm: 0.60 (td, *J* = 12.9, 3.5 Hz, 2H), 0.90 (s, 6H), 1.02–1.52 (m, 11*H*), 1.54–2.08 (m, 13H), 2.26–2.39 (m, 2H), 2.58–2.76 (m, 4H), 2.92 (br t, *J* = 6.3 Hz, 4H), 3.62 (s, 2H), 4.36 (br t, *J* = 6.3 Hz, 4H), 5.05 (s, 2H), 6.38 (d, *J* = 2.4 Hz, 2H), 6.44 (dd, *J* = 8.2, 2.4 Hz, 2H), 6.89 (d, *J* = 8.6 Hz, 2H), 7.08–7.23 (m, 5H), 7.84 (s, 2H), 8.93 (s, 2H); Fig. S14. **^{13}C NMR** (101 MHz, DMSO-d_6) δ ppm: 14.8, 24.0, 26.5, 27.6, 29.7, 33.1, 37.7, 43.6, 47.1, 47.7, 48.0, 53.3, 57.8, 81.6, 113.1, 115.3, 123.4, 126.4, 127.3, 128.5, 128.8, 130.8, 137.6, 139.2, 154.4, 155.3; Fig. S15. **HRMS-ESI**: calcd 837.49415 Da, found *m/z* 838.50126 $[M + H]^+$ and 860.48328 $[M + Na]^+$; Fig. S16. $[\alpha]_D^{28}$ = +46.8 (*c* = 0.25, DMF-$CHCl_3$, 1:1). **HPLC**: R_T = 7.855 min; Fig. S17.

(17β,17′β)-17,17′-{[(4-Methoxybenzyl)imino]bis(ethane-2,1-diyl-1*H*-1,2,3-triazole-1,4-diyl)}bisestra-1,3,5(10)-triene-3,17-diol (**D5**).

In reaction: **L5** (100 mg, 0.36 mmol), **EE** (234 mg, 0.79 mmol), $CuSO_4{\cdot}5H_2O$ (20 mg, 0.08 mmol), sodium ascorbate (24 mg, 0.12 mmol), DMF (8 mL). Chromatography with $CHCl_3$-MeOH 10:1 (*v/v*). Compound **D5** (190 mg, 0.22 mmol) was obtained as a white solid in 61 % yield. $\mathbf{R_F}$ = 0.2 in DCM-MeOH 10:1 (*v/v*). **^{1}H NMR** (400 MHz, DMSO-d_6) δ ppm: 0.61 (td, *J* = 12.8, 3.7 Hz, 2H), 0.92 (s, 6 H), 1.10–1.52 (m, 11*H*), 1.54–2.07 (m, 12H), 2.28–2.40 (m, 2 H), 2.59–2.77 (m, 4 H), 2.92 (br t, *J* = 6.3 Hz, 4 H), 3.49–3.59 (m, 2 H), 3.62 (s, 3 H), 4.36 (br t, *J* = 6.5 Hz, 4 H), 5.07 (s, 2 H), 6.40 (d, *J* = 2.4 Hz, 2 H), 6.45 (dd, *J* = 8.2, 2.4 Hz, 2 H), 6.75 (d, *J* = 8.6 Hz, 2 H), 6.90 (d, *J* = 8.6 Hz, 2 H), 7.03 (d, *J* = 8.6 Hz, 1 H), 7.85 (s, 2 H), 8.95 (s, 2 H); Fig. S18. **^{13}C NMR** (101 MHz, DMSO-d_6) δ ppm: 14.8, 24.0, 26.5, 27.6, 29.7, 33.1, 37.7, 43.6, 47.1, 47.7, 48.0, 53.1, 55.2, 57.2, 81.6, 113.1, 113.9, 115.3, 123.3, 126.4, 130.0, 130.8, 130.9, 137.6, 154.4, 155.3, 158.6; Fig. S19. **HRMS-ESI**: calcd 867.50472 Da, found *m/z* 868.51186 $[M + H]^+$, 890.49345 $[M + Na]^+$ and 906.46701 $[M + K]^+$; Fig. S20. $[\alpha]_D^{28}$ = +43.6 (*c* = 0.25, DMF-$CHCl_3$, 1:1). **HPLC**: R_T = 7.797 min; Fig. S21.

(17β,17′β)-17,17′-{[(3-Methoxybenzyl)imino]bis(ethane-2,1-diyl-

1*H*-1,2,3-triazole-1,4-diyl)}bisestra-1,3,5(10)-triene-3,17-diol (**D6**).

In reaction: **L6** (100 mg, 0.36 mmol), **EE** (234 mg, 0.79 mmol), $CuSO_4{\cdot}5H_2O$ (20 mg, 0.08 mmol), sodium ascorbate (24 mg, 0.12 mmol), DMF (8 mL). Chromatography with $CHCl_3$-MeOH 10:1 (*v/v*). Compound **D6** (260 mg, 0.3 mmol) was obtained as a white solid in 83 % yield. $\mathbf{R_F}$ = 0.2 in DCM-MeOH 10:1 (*v/v*). **^{1}H NMR** (400 MHz, DMSO-d_6) δ ppm: 0.60 (td, *J* = 12.7, 3.5 Hz, 2H), 0.91 (s, 6H), 1.11–1.50 (m, 10*H*), 1.56–2.07 (m, 10*H*), 2.28–2.40 (m, 2H), 2.59–2.77 (m, 4H), 2.94 (br t, *J* = 6.7 Hz, 4H), 3.55–3.65 (m, 2H), 3.68 (s, 3H), 4.36 (br t, *J* = 6.5 Hz, 4H), 5.05 (s, 2H), 6.40 (d, *J* = 2.4 Hz, 2H), 6.45 (dd, *J* = 8.4, 2.5 Hz, 2H), 6.69–6.76 (m, 2H), 6.78 (s, 1H), 6.90 (d, *J* = 8.2 Hz, 2H), 7.12 (t, *J* = 7.8 Hz, 1H), 7.86 (s, 2H), 8.95 (s, 2H); Fig. S22. **^{13}C NMR** (101 MHz, DMSO-d_6) δ ppm: 14.8, 24.0, 26.5, 27.6, 29.7, 33.1, 37.7, 43.6, 47.1, 47.8, 48.0, 53.4, 55.3, 57.8, 81.6, 112.9, 113.1, 114.3, 115.3, 121.0, 123.2, 126.4, 129.5, 130.8, 137.6, 140.9, 154.5, 155.3, 159.6; Fig. S23. **HRMS-ESI**: calcd 867.50472 Da, found *m/z* 868.51199 $[M + H]^+$, 890.49372 $[M + Na]^+$ and 906.46604 $[M + K]^+$; Fig. S24. $\mathbf{[\alpha]_D^{28}}$ = +48.8 (*c* = 0.25, DMF-$CHCl_3$, 1:1). **HPLC**: R_T = 7.858 min; Fig. S25.

(17β,17′β)-17,17′-{[(2,3-dimethoxybenzyl)imino]bis(ethane-2,1-diyl-1*H*-1,2,3-triazole-1,4-diyl)}bisestra-1,3,5(10)-triene-3,17-diol (**D7**).

In reaction: **L7** (100 mg, 0.33 mmol), **EE** (213 mg, 0.72 mmol), $CuSO_4{\cdot}5H_2O$ (17 mg, 0.07 mmol), sodium ascorbate (21 mg, 0.11 mmol), DMF (8 mL). Chromatography with $CHCl_3$-MeOH 10:1 (*v/v*). Compound **D7** (264 mg, 0.29 mmol) was obtained as a white solid in 88 % yield. $\mathbf{R_F}$ = 0.2 in DCM-MeOH 10:1 (*v/v*). **^{1}H NMR** (400 MHz, DMSO-d_6) δ ppm: 0.91 (s, 6H), 1.08–1.51 (m, 12H), 1.55–2.06 (m, 14H), 2.28–2.38 (m, 2 H), 2.60–2.72 (m, 4 H), 2.94 (br t, *J* = 6.5 Hz, 4 H), 3.64 (s, 3 H), 3.66 (s, 2 H), 3.73 (s, 3 H), 4.37 (br t, *J* = 6.5 Hz, 4 H), 5.05 (s, 2 H), 6.39 (d, *J* = 2.4 Hz, 2 H), 6.45 (dd, *J* = 8.4, 2.5 Hz, 2 H), 6.68 (dd, *J* = 7.2, 1.8 Hz, 1 H), 6.85–6.93 (m, 4 H), 7.85 (s, 2 H), 8.95 (s, 2 H); Fig. S26. **^{13}C NMR** (101 MHz, DMSO-d_6) δ ppm: 14.8, 24.0, 26.5, 27.6, 29.7, 33.1, 37.7, 43.6, 47.1, 47.9, 48.0, 51.7, 53.6, 55.9, 60.6, 81.6, 111.9, 113.1, 115.3, 121.9, 123.3, 124.1, 126.4, 130.8, 132.3, 137.6, 147.4, 152.7, 154.4, 155.3; Fig. S27. **HRMS-ESI**: calcd 897.51528 Da, found *m/z* 898.52256 $[M + H]^+$, 920.50447 $[M + Na]^+$ and 936.47639 $[M + K]^+$; Fig. S28. $\mathbf{[\alpha]_D^{27}}$ = +47.4 (*c* = 0.27, DMF-$CHCl_3$, 1:1). **HPLC**: R_T = 7.809 min; Fig. S29.

(17β,17′β)-17,17′-{[(3,4-Dimethoxybenzyl)imino]bis(ethane-2,1-diyl-1*H*-1,2,3-triazole-1,4-diyl)}bisestra-1,3,5(10)-triene-3,17-diol (**D8**).

In reaction: **L8** (100 mg, 0.33 mmol), **EE** (213 mg, 0.72 mmol), $CuSO_4{\cdot}5H_2O$ (17 mg, 0.07 mmol), sodium ascorbate (21 mg, 0.11 mmol), DMF (8 mL). Chromatography with $CHCl_3$-MeOH 10:1(*v/v*). Compound **D8** (281 mg, 0.31 mmol) was obtained as a white solid in 94 % yield. $\mathbf{R_F}$ = 0.2 in DCM-MeOH 10:1 (*v/v*). **^{1}H NMR** (400 MHz, DMSO-d_6) δ ppm: 0.58 (td, *J* = 12.8, 3.7 Hz, 2H), 0.90 (s, 6 H), 1.08–1.51 (m, 12H), 1.54–2.04 (m, 13H), 2.29–2.39 (m, 2 H), 2.60–2.77 (m, 4 H), 2.93 (br t, *J* = 6.7 Hz, 4 H), 3.60 (s, 3 H), 3.73 (s, 3 H), 4.35 (br t, *J* = 6.3 Hz, 4 H), 5.06 (s, 2 H), 6.39 (d, *J* = 2.4 Hz, 2 H), 6.44 (dd, *J* = 8.6, 2.4 Hz, 2 H), 6.64 (dd, *J* = 8.0, 1.4 Hz, 1 H), 6.70–6.74 (m, 1 H), 6.82 (d, *J* = 1.57 Hz, 1 H), 6.88 (d, *J* = 8.6 Hz, 2 H), 7.87 (s, 2 H), 8.95 (s, 2 H); Fig. S30. **^{13}C NMR** (101 MHz, DMSO-d_6) δ ppm: 14.8, 22.5, 24.0, 26.5, 27.6, 29.7, 31.4, 33.1, 37.6, 43.5, 47.1, 47.9, 47.9, 53.3, 55.6, 55.8, 57.6, 81.6, 111.5, 112.6, 113.0, 115.3, 120.8, 123.2, 126.4, 130.8, 131.5, 137.6, 148.1, 149.0, 154.5, 155.3; Fig. S31. **HRMS-ESI**: calcd 897.51528 Da, found *m/z* 898.52251 $[M + H]^+$, 920.50437 $[M + Na]^+$ and 936.47709 $[M + K]^+$; Fig. S32. $\mathbf{[\alpha]_D^{27}}$ = +41.5 (*c* = 0.26, DMF-$CHCl_3$, 1:1). **HPLC**: R_T = 7.652 min; Fig. S33.

(17β,17′β)-17,17′-{[(3,4-Dimethoxybenzyl)imino]bis(ethane-2,1-diyl-1*H*-1,2,3-triazole-1,4-diyl)}bisestra-1,3,5(10)-triene-3,17-diol (**D9**).

In reaction: **L9** (100 mg, 0.34 mmol), **EE** (223 mg, 0.76 mmol), $CuSO_4{\cdot}5H_2O$ (17 mg, 0.07 mmol), sodium ascorbate (21 mg, 0.11 mmol), DMF (8 mL). Chromatography with $CHCl_3$-MeOH 40:1 → 20:1 → 15:1 (*v/v*). Compound **D9** (266 mg, 0.3 mmol) was obtained as a white solid in 88 % yield. $\mathbf{R_F}$ = 0.6 in DCM-MeOH 10:1 (*v/v*). **^{1}H NMR** (400 MHz, DMSO-d_6) δ ppm: 0.61 (td, *J* = 12.7, 3.1 Hz, 2H), 0.91 (s, 6 H), 1.11–1.52 (m, 12H), 1.54–2.08 (m, 13H), 2.28–2.40 (m, 2 H), 2.60–2.76 (m, 4 H), 2.91 (br t, *J* = 6.5 Hz, 4 H), 3.51 (s, 2 H), 3.65 (s, 3 H), 4.34 (br t, *J* = 6.5 Hz, 4 H), 5.07 (s, 2 H), 6.39 (d, *J* = 2.4 Hz, 2 H), 6.45 (dd, *J* = 8.4, 2.5 Hz, 2 H), 6.52 (dd, *J* = 8.2, 2.0 Hz, 1 H), 6.66 (d, *J* = 1.6 Hz, 1 H), 6.72 (d, *J* = 8.2 Hz, 1 H), 6.91 (d, *J* = 8.61 Hz, 2 H), 7.85 (s, 2 H), 8.80 (s, 1 H), 8.95 (s, 2 H); Fig. S34. **^{13}C NMR** (101 MHz, DMSO-d_6) δ ppm: 14.8, 24.0, 26.5, 27.6, 29.7, 33.1, 37.7, 43.6, 47.1, 47.8, 48.0, 53.3, 55.9, 81.6, 112.2, 113.1, 115.3, 116.5, 119.6, 123.3, 126.4, 130.9, 131.4, 137.6, 146.6, 147.0, 154.4, 155.3; Fig. S35. **HRMS-ESI**: calcd 883.49963 Da, found *m/z* 884.50653 $[M + H]^+$, 906.48840 $[M + Na]^+$ and 922.46112 $[M + K]^+$; Fig. S36. $\mathbf{[\alpha]_D^{27}}$ = +50.0 (*c* = 0.26, DMF-$CHCl_3$, 1:1). **HPLC**: R_T = 7.576 min; Fig. S37.

(17β,17′β)-17,17′-{[(3-Hydroxy-4-methoxybenzyl)imino]bis(ethane-2,1-diyl-1*H*-1,2,3-triazole-1,4-diyl)}bisestra-1,3,5(10)-triene-3,17-diol (**D10**).

In reaction: **L10** (100 mg, 0.34 mmol), **EE** (223 mg, 0.76 mmol), $CuSO_4{\cdot}5H_2O$ (17 mg, 0.07 mmol), sodium ascorbate (21 mg, 0.11 mmol), DMF (8 mL). Chromatography with $CHCl_3$-MeOH 20:1 → 10:1 (*v/v*). Compound **D10** (253 mg, 0.29 mmol) was obtained as a white solid in 85 % yield. $\mathbf{R_F}$ = 0.5 in DCM-MeOH 10:1 (*v/v*). **^{1}H NMR** (400 MHz, DMSO-d_6) δ ppm: 0.60 (td, *J* = 12.6, 3.3 Hz, 2H), 0.91 (s, 6 H), 1.07–1.53 (m, 12H), 1.55–2.11 (m, 13H), 2.28–2.39 (m, 2 H), 2.58–2.78 (m, 4 H), 2.91 (br t, *J* = 6.5 Hz, 4 H), 3.54 (br s, 2 H), 3.73 (s, 3 H), 4.33 (br t, *J* = 6.3 Hz, 4 H), 5.05 (s, 2 H), 6.39 (d, *J* = 2.4 Hz, 2 H), 6.45 (dd, *J* = 8.4, 2.5 Hz, 2 H), 6.55 (br dd, *J* = 8.0, 1.4 Hz, 1 H), 6.60–6.65 (m, 1 H), 6.79 (d, *J* = 1.2 Hz, 1 H), 6.91 (br d, *J* = 8.6 Hz, 2 H), 7.83–7.88 (m, 2 H), 8.79 (s, 1 H), 8.94 (s, 2 H); Fig. S38. **^{13}C NMR** (101 MHz, DMSO-d_6) δ ppm: 14.8, 24.0, 26.5, 27.6, 29.7, 33.1, 37.7, 43.6, 47.1, 47.8, 48.0, 53.3, 56.0, 81.6, 113.1, 115.3, 121.3, 123.2, 126.4, 129.8, 130.8, 137.6, 145.9, 147.8, 154.5, 155.3; Fig. S39. **HRMS-ESI**: calcd 883.49963 Da, found *m/z* 884.50654 $[M + H]^+$, 906.48847 $[M + Na]^+$ and 922.46096 $[M + K]^+$; Fig. S40. $\mathbf{[\alpha]_D^{28}}$ = +33.2 (*c* = 0.25, DMF-$CHCl_3$, 1:1). **HPLC**: R_T = 7.504 min; Fig. S41.

(17β,17′β)-17,17′-{[(3,4,5-Trimethoxybenzyl)imino]bis(ethane-2,1-diyl-1*H*-1,2,3-triazole-1,4-diyl)}bisestra-1,3,5(10)-triene-3,17-diol (**D11**).

In reaction: **L11** (100 mg, 0.3 mmol), **EE** (194 mg, 0.66 mmol), $CuSO_4{\cdot}5H_2O$ (17 mg, 0.07 mmol), sodium ascorbate (21 mg, 0.11 mmol), DMF (8 mL). Chromatography with $CHCl_3$-MeOH 25:1 (*v/v*). Compound **D11** (250 mg, 0.27 mmol) was obtained as a white solid in 90 % yield. $\mathbf{R_F}$ = 0.5 in DCM-MeOH 10:1 (*v/v*). **^{1}H NMR** (400 MHz, DMSO-d_6) δ ppm: 0.57 (td, *J* = 12.8, 3.3 Hz, 2H), 0.90 (s, 6 H), 1.10–1.48 (m, 12H), 1.55–2.02 (m, 13H), 2.27–2.38 (m, 2 H), 2.61–2.75 (m, 4 H), 2.94 (br t, *J* = 5.7 Hz, 4 H), 3.53 (s, 3 H), 3.73 (s, 6 H), 4.36 (br t, *J* = 6.7 Hz, 3 H), 5.05 (s, 2 H), 6.39 (d, *J* = 2.4 Hz, 2 H), 6.44 (dd, *J* = 8.4, 2.5 Hz, 2 H), 6.53 (s, 2 H), 6.87 (d, *J* = 8.6 Hz, 2 H), 7.88 (s, 2 H), 8.94 (s, 2 H); Fig. S42. **^{13}C NMR** (101 MHz, DMSO-d_6) δ ppm: 14.8, 24.0, 26.5, 27.6, 29.7, 33.1, 37.6, 43.5, 47.1, 47.9, 53.5, 56.2, 60.2, 81.6, 105.9, 113.0, 115.3, 123.1, 126.4, 130.8, 134.9, 136.6, 137.5, 153.1, 154.6, 155.3; Fig. S43. **HRMS-ESI**: calcd 927.52585 Da, found *m/z* 928.53309 $[M + H]^+$, 950.51508 $[M + Na]^+$ and 966.48715 $[M + K]^+$; Fig. S44. $\mathbf{[\alpha]_D^{28}}$ = +38.1 (*c* = 0.26, DMF-$CHCl_3$, 1:1). **HPLC**: R_T = 7.782 min; Fig. S45.

(17β,17′β)-17,17′-{[(2,3,4-Trimethoxybenzyl)imino]bis(ethane-2,1-diyl-1*H*-1,2,3-triazole-1,4-diyl)}bisestra-1,3,5(10)-triene-3,17-diol (**D12**).

In reaction: **L12** (100 mg, 0.3 mmol), **EE** (194 mg, 0.66 mmol), $CuSO_4{\cdot}5H_2O$ (17 mg, 0.07 mmol), sodium ascorbate (21 mg, 0.11 mmol), DMF (8 mL). Chromatography with $CHCl_3$-MeOH 25:1(*v/v*). Compound **D12** (220 mg, 0.24 mmol) was obtained as a white solid in 80 % yield. $\mathbf{R_F}$ = 0.4 in DCM-MeOH 10:1 (*v/v*). **^{1}H NMR** (400 MHz, DMSO-d_6) δ ppm: 0.60 (td, *J* = 12.9, 3.9 Hz, 2H), 0.91 (s, 6 H), 1.10–1.52 (m, 12H), 1.55–2.09 (m, 10*H*), 2.25–2.41 (m, 2 H), 2.56–2.77 (m, 4 H), 2.93 (br t, *J* = 6.7 Hz, 4 H), 3.55–3.63 (s, 2 H), 3.67 (s, 3 H),

3.68 (s, 3 H), 3.70 (s, 3 H), 4.36 (br t, $J = 6.7$ Hz, 4 H), 5.05 (s, 2 H), 6.39 (d, $J = 2.4$ Hz, 2 H), 6.44 (dd, $J = 8.2$, 2.4 Hz, 2 H), 6.61 (d, $J = 8.6$ Hz, 1 H), 6.76 (d, $J = 8.6$ Hz, 1 H), 6.91 (d, $J = 8.61$ Hz, 2 H), 7.85 (s, 2 H), 8.95 (s, 2 H); Fig. S46. **^{13}C NMR** (101 MHz, DMSO-d_6) δ ppm: 14.8, 24.0, 26.5, 27.6, 29.7, 33.1, 37.6, 43.6, 47.1, 47.8, 48.0, 51.7, 53.5, 56.0, 60.7, 61.3, 81.6, 107.9, 113.1, 115.3, 123.3, 124.2, 124.7, 126.4, 130.8, 137.6, 142.0, 152.2, 152.8, 154.4, 155.3; Fig. S47. **HRMS-ESI**: calcd 927.52585 Da, found *m/z* 928.53317 $[M + H]^+$, 950.51524 $[M + Na]^+$ and 966.48676 $[M + K]^+$; Fig. S48. **$[\alpha]_D^{28}$** = +41.9 ($c = 0.26$, DMF-$CHCl_3$, 1:1). **HPLC**: $R_T = 7.647$ min; Fig. S49.

(17β,17′β)-17,17′-[Oxybis(ethane-2,1-diyloxyethane-2,1-diyl-1*H*-1,2,3-triazole-1,4-diyl)]bisestra-1,3,5(10)-triene-3,17-diol (**D13**).

In reaction: **L13** (50 mg, 0.2 mmol), **EE** (133 mg, 0.45 mmol), $CuSO_4{\cdot}5H_2O$ (11.2 mg, 0.045 mmol), sodium ascorbate (13 mg, 0.068 mmol), DMF (3 mL). Chromatography with $CHCl_3$-MeOH 25:1 → 10:1 (*v/v*). Compound **D13** (99 mg, 0.12 mmol) was obtained as a white solid in 59 % yield. $\mathbf{R_F} = 0.43$ in DCM-MeOH 10:1 (*v/v*). **^{1}H NMR** (400 MHz, DMSO-d_6) δ ppm: 0.59 (td, $J = 12.6$, 3.3 Hz, 2H), 0.91 (s, 6 H), 1.14–2.10 (m, 22H), 2.30–2.41 (m, 4 H), 2.62–2.72 (m, 4 H), 3.43–3.53 (m, 8 H), 3.79 (t, $J = 5.3$ Hz, 4 H), 4.49 (t, $J = 5.3$ Hz, 4 H), 5.10 (s, 2 H), 6.41 (d, $J = 2.4$ Hz, 2 H), 6.46 (dd, $J = 8.2$, 2.4 Hz, 2 H), 6.93 (d, $J = 8.6$ Hz, 2 H), 7.82 (s, 2 H), 8.98 (s, 2 H); Fig. S50. **^{13}C NMR** (101 MHz, DMSO-d_6) δ ppm: 14.83, 24.00, 26.51, 27.64, 29.70, 33.05, 37.57, 43.62, 47.10, 47.94, 49.62, 69.31, 69.97, 70.14, 81.51, 113.08, 115.31, 123.43, 126.40, 130.80, 137.57, 154.37, 155.31; Fig. S51. **HRMS-ESI**: calcd 836.48365 Da, found *m/z* 837.49030 $[M + H]^+$, 859.47229 $[M + Na]^+$ and 875.44519 $[M + K]^+$; Fig. S52. **$[\alpha]_D^{20}$**=+56.8 ($c = 0.25$, DMF-$CHCl_3$, 1:1). **HPLC**: $R_T = 9.109$ min; Fig. S53.

4.2. Biochemistry

4.2.1. Cell lines

CCRF-CEM, K562, U2OS, A549, MRC-5 and BJ cell lines were purchased from American Tissue Culture Collection (ATCC) HCT116 and HCT116p53-/-cell lines were obtained from Horizon Discovery. Resistant CEM-DNR bulk cell line overexpressing MRP-1 and P-glycoprotein and K562-TAX subline expressing P-glycoprotein were selected by increasing doses of daunorubicin or paclitaxel [17]. Cells were cultured in the humidified incubator under the atmosphere of 95 % air and 5 % CO_2 at 37 °C according to the supplier's recommendations. The cell culture medium DMEM/RPMI 1640 (Lonza) was supplemented with 100 U/mL penicillin, 100 mg/mL streptomycin and 10 % fetal bovine serum (Gibco).

4.2.2. MTS assay

Cells were seeded into 384-well microtiter plates and incubated overnight. The next day, the treatment in dose–response was performed using Echo550 acoustic liquid handler (Labcyte). The plates were incubated for 72 h in a humidified CO_2 incubator and then treated with 3-(4,5-dimethylthiazol-2-yl)-5-(3-carboxymethoxyphenyl)-2-(4-sulfophenyl)–2*H*-tetrazolium (MTS) and phenazine methosulfate solution. The absorbance of the reduced substrate was measured at 490 nm using EnVision multilabel plate reader (PerkinElmer) after an additional 2-hour incubation. The IC_{50} value was calculated from the appropriate dose − response curves using Dotmatics Studies software.

4.2.3. FACS analysis

The cell cycle analysis and immunolabeling of cell cycle markers were described previously [18]. Briefly, CCRF-CEM were incubated with compounds for 24 h, then harvested, washed with cold phosphate-buffered saline (PBS), fixed in cold 70 % ethanol, treated with RNase (0.5 mg/mL) and stained with propidium iodide (PI) (0.1 mg/mL). The data were acquired using FACSCalibur (Becton Dickinson) and analyzed in the program ModFitLT (Verity). Apoptosis was measured in logarithmic mode as a percentage of the particles with PI content lower than cells in G0/G1 phase (<G0/G1) of the cell cycle and polyploidy was measured in linear mode as a percentage of particles with PI content higher than cells in G2/M phase of the cell cycle. To assess the rate of DNA and RNA synthesis the cells were incubated with compounds for 24 h and pulse-labelled with 5-bromo-2-deoxyuridine (BrdU) or 5-bromouridine (BrU) for 30 min. BrDU, as well as BrU, are recognized by anti-BrdU antibody clone MoBu-1 (Exbio). As a mitotic marker was used anti-phospho-Histone H3 (Ser10) antibody (Merck Millipore). All above-mentioned primary antibodies were diluted in blocking buffer and used with secondary anti-mouse-FITC-conjugated antibody (Sigma-Aldrich). Following the labelling, cells were washed with PBS and incubated with 0.1 mg/mL propidium iodide and 0.5 mg/mL RNase A for 1 h and analyzed by flow cytometry using a 488 nm single beam laser (FACS-Calibur, Becton Dickinson). Data analysis was performed using Cell-Quest software.

4.2.4. Tubulin polymerization assay

Tubulin polymerization assay (Cytoskeleton) was performed according to the manufacturer's protocol. The assay is based on the analysis of light scattering by polymerized tubulin (>99 % purity) in the reaction. The absorbance of polymerized porcine brain tubulin was measured using EnVision Multilabel Plate Reader (PerkinElmer) at 37 °C in the presence of 10 μmol/L compounds or DMSO. Polymerization curves were used for the calculation of the maximal velocity of polymerization values (V_{max}).

4.2.5. Immunofluorescence

U2OS cells were seeded onto coverslips and after overnight incubation with compounds were washed in PBS and fixed in 3 % paraformaldehyde and 10 mM MES, 150 mM NaCl, 5 mM EGTA, 5 mM $MgCl_2$, 5 mM glucose (pH 6.1). Alternatively, the compounds were removed from the cells by three PBS washouts, then incubated in a fresh cultivation medium for 30 min at 37 °C, washed in PBS and fixed in 3 % paraformaldehyde. Cell permeabilization was performed using 0.3 % Triton X-100 in PBS and nuclei were visualized using Hoechst 33342. Following the 1-hour blocking with 1 % bovine serum albumin in PBS (Sigma-Aldrich) samples were incubated for 60 min with α-tubulin mouse monoclonal antibody (Sigma-Aldrich) in PBS containing 1 % BSA and 0.3 % Triton X-100. For visualization were used Alexa Fluor-488 conjugated anti-mouse antibodies were (Life Technologies). The samples were washed three times in PBS for 5 min and mounted with Vectashield Mounting Medium. Images were acquired using a spinning disk confocal microscope (Zeiss) with a CSU-X1 unit (Yokogawa).

5. *In silico* modelling

For this study, the 3D complex (4O2B) of bovine tubulin alpha 1B (P81947) and beta-2B (Q6B856) chains with the known inhibitor colchicine were considered. We removed water molecules and native inhibitors from the structures. 3D structure of the unresolved residues was rebuilt by Modeller Tool [19] built-in Chimera [20]. Remodelling of incomplete side chains and protonation of the protein structure was performed by Chimera Dock Prep tool [20]. GTP molecule and Mg^{2+} ion nearby the active site are reported to be important for the regulation of the polymerization thereby these crucial cofactors were kept.

5.1. Molecular docking

All compounds were docked using Autodock Vina [21]. Due to the large size of estradiol dimer molecules, we used a large docking box with a size of 28 × 28 × 28 Å centred around the active site. To provide reasonable accuracy and efficiency the exhaustiveness value was set to 32. Initial conformers were obtained by RDKit 2018.09.1.0 version [22]. Ligand protonation was performed by Marvin cxcalc utility for pH 7.4 (ref. [23]).

5.2. Molecular dynamics

We used GROMACS software version 2021.4-plumed-2.7.3 (ref. [24,25]). For target preparation, we used the Amber 99SB-ILDN force field [26] and the TIP3P water model. Na and Cl ions were added to neutralize the system. Ligand topologies were prepared by AmberTools version 20.9 (ref. [27]). Energy minimization for every simulation took 50,000 steps, followed by NVT and then NPT equilibrations for 1000 ps. Production simulations were conducted for 150 ns in an NPT ensemble at 300 K. For the visualization and analysis of the protein–ligand interaction we used ProLIF package [13] using only frames extracted from the last 100 ns.

5.3. Calculation of binding free energy with MM-PBSA

MM/PBSA models were generated using gmx_MMPBSA [28,29]. The Amber99SB-ILDN force field was used to calculate the internal term (ΔE_{int}) as well as van der Waals (ΔE_{vdW}) and electrostatic (ΔE) energies. The last 10 ns (1001 frames) from the full 150 ns simulations were used for the binding free energy estimation. The entropic term was calculated by the Interaction Entropy (IE) method [30]. The temperature for IE analysis was set to 298.00 K. IE was calculated using the last quartile (seg = 25) of the last 10 ns (251 frames). The ion strength option (istrng) was set to 150 mM, a typical value for a physiological environment. Atomic radii from the topology files were used (radiopt = 0). Considering charged environment of the active site the internal dielectric constant value (indi) was set to 4 ref. [31]. Other variables of the MM/PBSA method were set by practical examples provided by gmx_MMPBSA or by the default. The full setup is provided in supplementary materials.

CRediT authorship contribution statement

Michal Jurášek: Conceptualization, Methodology, Writing – original draft. **Jiří Řehulka:** Formal analysis, Methodology, Writing – original draft. **Lenka Hrubá:** synthesis, analytical characterizations. **Aleksandra Ivanová:** *in silico* modelling. **Soňa Gurská:** biological experiments. **Olena Mokshyna:** *in silico* modelling. **Pavel Trousil:** synthesis, analytical characterizations. **Lukáš Huml:** synthesis, analytical characterizations. **Pavel Polishchuk:** Formal analysis, Software, Writing – original draft. **Marián Hajdúch:** Supervision, Conceptualization, Writing – review & editing. **Pavel B. Drašar:** Supervision, Writing – review & editing, designed molecules. **Petr Džubák:** Supervision, Writing – review & editing, designed biological experiments, biological experiments.

Declaration of Competing Interest

The authors declare that they have no known competing financial interests or personal relationships that could have appeared to influence the work reported in this paper.

Data availability

Data will be made available on request.

Acknowledgement

This work is dedicated to the memory of Ing. Pavel Trousil, who was a highly talented young scientist and who participated in the creation of this work within his master thesis. This work was supported by CEREBIT (Project No. CZ.02.1.01/0.0/0.0/16_025/0007397), an internal grant of the UCT Prague No. A1_FPBT_2022_007 and by the Ministry of Education, Youth and Sports of the Czech Republic through the e-INFRA CZ (ID:90140), infrastructural projects (CZ-OPENSCREEN – LM2018130; EATRIS-CZ – LM2018133) and National Institute for Cancer Research (Programme EXCELES, ID Project No. LX22NPO5102) - Funded by the European Union - Next Generation EU.

Appendix A. Supplementary data

Supplementary data to this article can be found online at https://doi.org/10.1016/j.bioorg.2022.106334.

References

[1] M. Jurášek, P. Džubák, D. Sedlák, H. Dvořáková, M. Hajdúch, P. Bartůněk, P. Drašar, Preparation, preliminary screening of new types of steroid conjugates and their activities on steroid receptors, Steroids 78 (3) (2013) 356–361.
[2] K. Battiston, I. Parrag, M. Statham, D. Louka, H. Fischer, G. Mackey, A. Daley, F. Gu, E. Baldwin, B. Yang, B. Muirhead, E.A. Hicks, H. Sheardown, L. Kalachev, C. Crean, J. Edelman, J.P. Santerre, W. Naimark, Polymer-free corticosteroid dimer implants for controlled and sustained drug delivery, Nat. Commun. 12 (1) (2021) 2875.
[3] D. Xu, C. Peng, F. Gao, Z. Guo, R. Zhuang, X. Su, X. Zhang, Radioiodinated estradiol dimer for estrogen receptor targeted breast cancer imaging, Chem. Biol. Drug. Des. 96 (6) (2020) 1332–1340.
[4] L. Nahar, S.D. Sarker, A review on steroid dimers: 2011–2019, Steroids 164 (2020), 108736.
[5] M. Jurášek, M. Černohorská, J. Řehulka, V. Spiwok, T. Sulimenko, E. Dráberová, M. Darmostuk, S. Gurská, I. Frydrych, R. Burianová, T. Ruml, M. Hajdúch, P. Bartůněk, P. Dráber, P. Džubák, P.B. Drašar, D. Sedlák, Estradiol dimer inhibits tubulin polymerization and microtubule dynamics, J. Steroid. Biochem. Mol. Biol. 183 (2018) 68–79.
[6] R. Huisgen, Kinetics and mechanism of 1,3-dipolar cycloadditions, Angew. Chem. Int. Ed. 2 (11) (1963) 633–645.
[7] I.J. Fairlamb, P.S. Bäuerlein, L.R. Marrison, J.M. Dickinson, Pd-catalysed cross coupling of terminal alkynes to diynes in the absence of a stoichiometric additive, Chem. Commun. 5 (2003) 632–633.
[8] N. Aguilar-Valdez, M. Maldonado-Domínguez, R. Arcos-Ramos, M. Romero-Ávila, R. Santillan, N. Farfán, Synthesis of steroidal molecular compasses: exploration of the controlled assembly of solid organic materials, CrystEngComm 19 (13) (2017) 1771–1777.
[9] D. Fournier, D. Poirier, Estradiol dimers as a new class of steroid sulfatase reversible inhibitors, Bioorg. Med. Chem. Lett. 19 (3) (2009) 693–696.
[10] D. Rabouin, V. Perron, B. N'Zemba, R. C.-Gaudreault, G. Bérubé, A facile synthesis of C2-symmetric 17β-estradiol dimers, Bioorg. Med. Chem. Lett. 13(3) (2003) 557-560.
[11] M. Cushman, H.M. He, J.A. Katzenellenbogen, R.K. Varma, E. Hamel, C.M. Lin, S. Ram, Y.P. Sachdeva, Synthesis of analogs of 2-methoxyestradiol with enhanced inhibitory effects on tubulin polymerization and cancer cell growth, J. Med. Chem. 40 (15) (1997) 2323–2334.
[12] J. Škubník, M. Jurášek, T. Ruml, S. Rimpelová, Mitotic poisons in research and medicine, Molecules 25 (20) (2020).
[13] C. Bouysset, S. Fiorucci, ProLIF: a library to encode molecular interactions as fingerprints, J. Cheminform. 13 (2021).
[14] L. Niu, J. Yang, W. Yan, Y. Yu, Y. Zheng, H. Ye, Q. Chen, L. Chen, Reversible binding of the anticancer drug KXO1 (tirbanibulin) to the colchicine-binding site of β-tubulin explains KXO1's low clinical toxicity, J. Biol. Chem. 294 (48) (2019) 18099–18108.
[15] J.R. Thomas, X.J. Liu, P.J. Hergenrother, Size-specific ligands for RNA hairpin loops, J. Am. Chem. Soc. 127 (36) (2005) 12434–12435.
[16] Y. Song, H. Zong, E.R. Trivedi, B.J. Vesper, E.A. Waters, A.G.M. Barrett, J. A. Radosevich, B.M. Hoffman, T.J. Meade, Synthesis and Characterization of New Porphyrazine-Gd(III) Conjugates as Multimodal MR Contrast Agents, Bioconjugate Chem. 21 (12) (2010) 2267–2275.
[17] V. Nosková, P. Džubák, G. Kuzmina, A. Ludková, D. Stehlík, R. Trojanec, A. Janoštáková, G. Kořínková, V. Mihal, M. Hajdúch, In vitro chemoresistance profile and expression/function of MDR associated proteins in resistant cell lines derived from CCRF-CEM, K562, A549 and MDA MB 231 parental cells, Neoplasma 49 (6) (2002) 418–425.
[18] A. Bourderioux, P. Nauš, P. Perlíková, R. Pohl, I. Pichová, I. Votruba, P. Džubák, P. Konečný, M. Hajdúch, K.M. Stray, T. Wang, A.S. Ray, J.Y. Feng, G. Birkus, T. Cihlář, M. Hocek, Synthesis and significant cytostatic activity of 7-hetaryl-7-deazaadenosines, J. Med. Chem. 54 (15) (2011) 5498–5507.
[19] A. Sali, T.L. Blundell, Comparative protein modelling by satisfaction of spatial restraints, J. Mol. Biol. 234 (3) (1993) 779–815.
[20] E.F. Pettersen, T.D. Goddard, C.C. Huang, G.S. Couch, D.M. Greenblatt, E.C. Meng, T.E. Ferrin, UCSF Chimera–a visualization system for exploratory research and analysis, J. Comput. Chem. 25 (13) (2004) 1605–1612.
[21] O. Trott, A.J. Olson, AutoDock Vina: improving the speed and accuracy of docking with a new scoring function, efficient optimization, and multithreading, J. Comput. Chem. 31 (2) (2010) 455–461.
[22] G. Landrum, RDKit, Open-Source Cheminformatics Software, 2021.
[23] Cxcalc utility was used for ligand protonation, Cxcalc version 19.22.0, ChemAxon (https://www.chemaxon.com).
[24] B. Hess, C. Kutzner, D. van der Spoel, E. Lindahl, GROMACS 4: Algorithms for highly efficient, load-balanced, and scalable molecular simulation, J. Chem. Theory. Comput. 4 (3) (2008) 435–447.

[25] S. Pronk, S. Pall, R. Schulz, P. Larsson, P. Bjelkmar, R. Apostolov, M.R. Shirts, J. C. Smith, P.M. Kasson, D. van der Spoel, B. Hess, E. Lindahl, GROMACS 4.5: a high-throughput and highly parallel open source molecular simulation toolkit, Bioinformatics 29 (7) (2013) 845–854.
[26] K. Lindorff-Larsen, S. Piana, K. Palmo, P. Maragakis, J.L. Klepeis, R.O. Dror, D. E. Shaw, Improved side-chain torsion potentials for the Amber ff99SB protein force field, Proteins 78 (8) (2010) 1950–1958.
[27] D.A. Case, T.E. Cheatham 3rd, T. Darden, H. Gohlke, R. Luo, K.M. Merz Jr., A. Onufriev, C. Simmerling, B. Wang, R.J. Woods, The Amber biomolecular simulation programs, J. Comput. Chem. 26 (16) (2005) 1668–1688.
[28] M.S. Valdes-Tresanco, M.E. Valdes-Tresanco, P.A. Valiente, E. Moreno, gmx_MMPBSA: A New Tool to Perform End-State Free Energy Calculations with GROMACS, J. Chem. Theory. Comput. 17 (10) (2021) 6281–6291.
[29] B.R. Miller 3rd, T.D. McGee Jr., J.M. Swails, N. Homeyer, H. Gohlke, A.E. Roitberg, MMPBSA.py: An Efficient Program for End-State Free Energy Calculations, J. Chem. Theory. Comput. 8 (9) (2012) 3314–3321.
[30] L. Duan, X. Liu, J.Z. Zhang, Interaction entropy: A new paradigm for highly efficient and reliable computation of protein-ligand binding free energy, J. Am. Chem. Soc. 138 (17) (2016) 5722–5728.
[31] T. Hou, J. Wang, Y. Li, W. Wang, Assessing the performance of the MM/PBSA and MM/GBSA methods. 1. The accuracy of binding free energy calculations based on molecular dynamics simulations, J. Chem. Inf. Model. 51 (1) (2011) 69–82.